International Journal of Geo-Information

MDPI

Article

Geospatial Multi-Hazard Assessment for Gyeonggi-do Province, South Korea Subjected to Earthquake

Han-Saem Kim [1] and Mingi Kim [2,*]

[1] Department of Civil and Energy System Engineering, Kyonggi University, Suwon 16227, Republic of Korea; hansaem@kyonggi.ac.kr
[2] Disaster Management Research Center, Seoul Institute, Seoul 06756, Republic of Korea
* Correspondence: mingikim@si.re.kr

Abstract: The increasing frequency of earthquake events worldwide, particularly in South Korea, necessitates detailed seismic hazard assessments to mitigate the risks to urban infrastructure. This study addresses this pressing need by developing a comprehensive multi-hazard assessment framework specific to the Gyeonggi-do Province. By leveraging advanced geospatial computation techniques and geographic information systems, this study integrated geotechnical data, terrain information, and building inventories to evaluate seismic site effects, earthquake-induced landslide hazards, and structural vulnerability. This method uses geostatistical methods to construct geotechnical spatial grids that correlate site-specific seismic responses to potential hazards. The key findings revealed significant variations in seismic site responses owing to local subsurface characteristics, emphasizing the importance of site-specific seismic hazard maps for urban disaster preparedness. The framework's effectiveness was validated by analyzing the 2017 Pohang earthquake, which demonstrated a strong correlation between predicted and observed damage. This study highlights the importance of ongoing seismic hazard assessment methodology development and advocates interdisciplinary collaboration to improve urban resilience, ultimately protecting communities from the impacts of future earthquakes.

Keywords: hazard map; seismic site effect; earthquake-induced landslide; seismic fragility function; geospatial analysis; Gyeonggi-do

check for updates

Citation: Kim, H.-S.; Kim, M. Geospatial Multi-Hazard Assessment for Gyeonggi-do Province, South Korea Subjected to Earthquake. *ISPRS Int. J. Geo-Inf.* **2024**, *13*, 439. https://doi.org/10.3390/ijgi13120439

Academic Editors: Wolfgang Kainz, Dimitrios D. Alexakis and Adrianos Retalis

Received: 10 September 2024
Revised: 21 November 2024
Accepted: 29 November 2024
Published: 5 December 2024

Copyright: © 2024 by the authors. Published by MDPI on behalf of the International Society for Photogrammetry and Remote Sensing. Licensee MDPI, Basel, Switzerland. This article is an open access article distributed under the terms and conditions of the Creative Commons Attribution (CC BY) license (https://creativecommons.org/licenses/by/4.0/).

1. Introduction

The frequency of earthquakes has increased worldwide, highlighting the urgent need for detailed seismic studies, particularly in South Korea. The growing number of seismic hazards, such as ground shaking, liquefaction, and landslides, presents a significant threat to structures situated on seismically vulnerable soils, necessitating the development of comprehensive site-specific seismic hazard maps. For this purpose, advanced geospatial computation techniques based on geotechnical hazards evaluations and visualization methods are crucial. To produce accurate hazard assessments, these techniques integrate composite geodata including geotechnical surveys and geological/terrain thematic maps [1]. Geospatial assessments of complex hazards caused by earthquakes have gained significant attention in recent years, particularly as urbanization and infrastructure development have increased seismic vulnerability events. A comprehensive review of the existing literature revealed several key themes and methodologies that contribute to our current understanding of seismic hazards and their impacts [2].

Seismic hazard assessments are heavily influenced by site-specific factors such as topography and soil dynamics. Effective evaluation of earthquake-triggered geotechnical disasters requires the implementation of comprehensive geodata systems. This method enables the prediction and analysis of seismic impacts based on detailed local conditions [3]. Large urban areas, such as Seoul and Gyeonggi-do, have significant spatial variability

in topography, ground quality, and geotechnical properties because of diverse urban developments and infrastructure. Therefore, a thorough assessment involves the integration of geological maps, land cover data, facility inventories (such as building and pipeline data), and sporadic geotechnical survey results [4]. Geographic information systems (GIS) are increasingly being used to manage and analyze this data to improve geotechnical property prediction across large areas [1,5,6].

Recent seismic events in South Korea, such as the Gyeongju earthquake (M_L 5.8, 2016) and the Pohang earthquake (M_L 5.4, 2017), have demonstrated damage variability across different areas, including localized regions. These events highlight the importance of conducting site-specific seismic assessments to better understand the differential impacts of earthquakes on infrastructure [7]. Previous studies have shown that local geological conditions have a significant influence on seismic site response [8–10]. For instance, the Newcastle earthquake (M_L 5.6, 1996) caused severe damage, predominantly in alluvial and landfill areas, because of the complex interactions between soil thickness, topography, and existing structures [11].

Landslides triggered by seismic activity are critical hazards. These events not only cause direct damage to structures but also disrupt vital infrastructure, such as roads and lifelines, affecting social systems. Despite the high risk, systematic research into earthquake-induced slope stability in South Korea is limited. This study aims to address this gap by developing GIS-based models for assessing landslide hazards, considering dynamic factors such as safety and Newmark displacement. These models will aid in understanding and mitigating the risks associated with slope stability during seismic events [12–14].

In terms of structural damage, effective seismic risk management and mitigation strategies are required. These strategies should include systematic methodologies that leverage computer-aided systems, such as GIS tools, to analyze and manage seismic vulnerability. The development of such systems involves generating geotechnical spatial grids, determining seismic loads on building sites, and evaluating structural fragility in real time. The integration of wireless network systems with seismometers can further improve these analyses by providing real-time data on seismic activity [15,16]. The proposed methodology includes constructing geotechnical spatial grids to estimate site-specific peak ground accelerations (PGAs), assessing structural damage by calculating failure probabilities, and integrating geotechnical data [17].

The integration of multiple hazard assessments, such as ground shaking, liquefaction, and landslides into a cohesive framework is critical for comprehensive disaster risk management. According to the literature, multi-hazard frameworks can improve urban disaster preparedness by providing a comprehensive view of potential risks and allowing for more effective response strategies [17]. This study presents a multi-hazard assessment framework developed specifically for the Gyeonggi-do Province, South Korea, with a focus on seismic impacts, landslide hazards, and structural vulnerability. By addressing these factors, this study aimed to provide a comprehensive tool for urban disaster preparedness and response, which is crucial for managing the risks associated with seismic activity in densely populated and industrially significant areas.

2. Macroscale Framework of Multi-Hazard Assessment Subjected to Earthquake

2.1. Framework Architecture

A computer-aided decision-making procedure for evaluating the macroscale seismic response and the resulting landslide and structural fragility in seismically vulnerable areas was proposed, consisting of three phases: (1) site-specific evaluation of the seismic site effect (Figure 1), (2) mapping of earthquake-induced landslide hazards, and (3) seismic impact analysis using structure fragility. For the spatial computation of earthquake-induced geohazards, an optimal evaluation and visualization scheme was developed using GIS-based multi-layer information to facilitate the linkage and visualization of layer information for each evaluation step based on the seismic hazard and vulnerability parameters. Prior to the major workflow, spatially correlated complex geospatial information, such as superstruc-

ture, terrain, subsurface, groundwater, and underground pipelines, was standardized using GIS-based data pre-processing and visualization techniques. In this study, multivariate rules represented by GIS layers were defined as geodata.

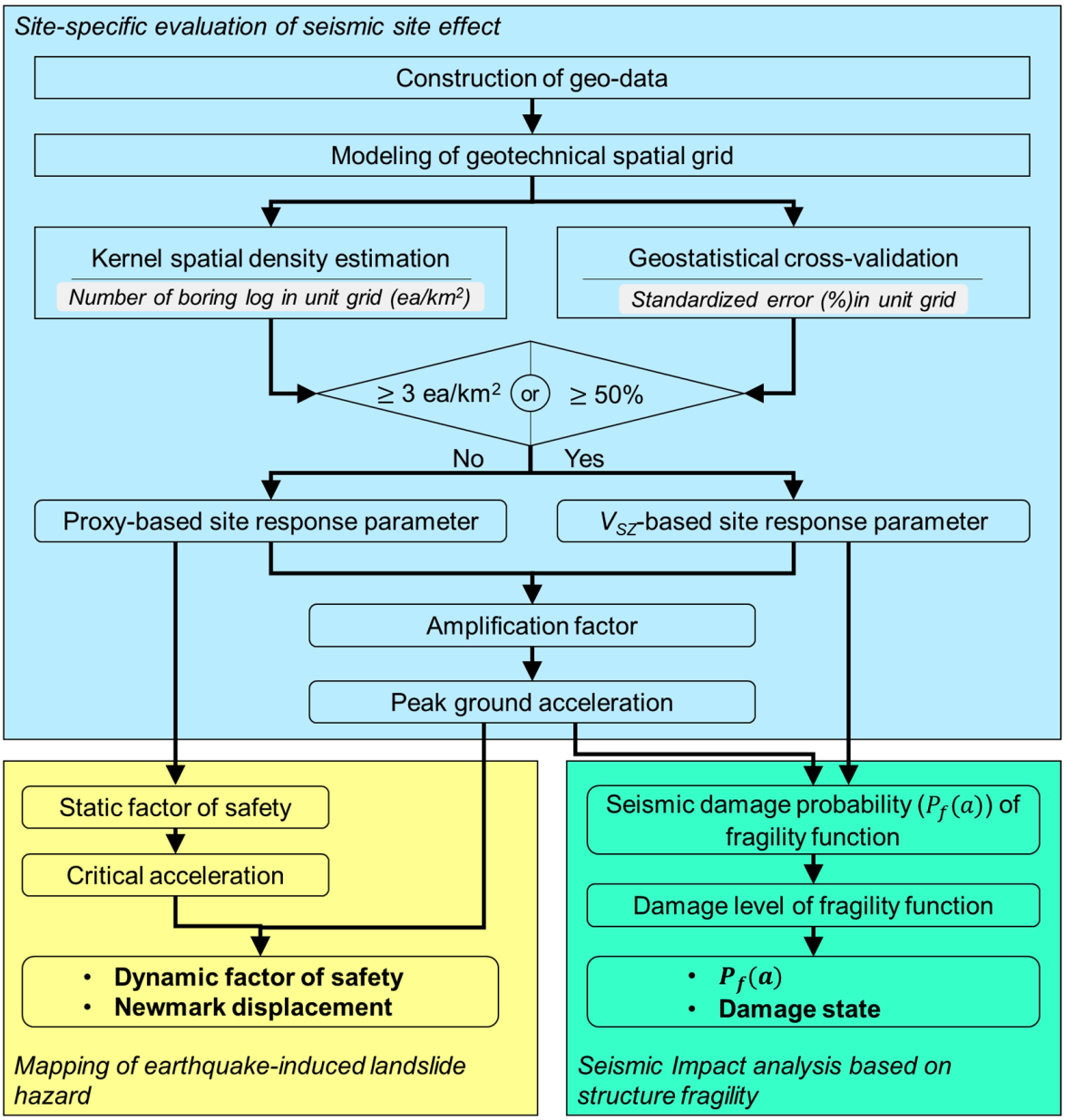


Figure 1. Computer-based framework architecture for macroscale multi-hazard zonation composed three phases (site-specific evaluation of seismic site effect, mapping of earthquake-induced landslide hazard, and seismic impact analysis based on structure fragility).

In the first phase, a geotechnical spatial grid was constructed using the geostatistical method, focusing on geotechnical characteristics, to provide site-specific response characteristics that could be correlated with landslides and structural fragility. Using the geotechnical spatial grid, correlations between the measured ground motion at the bedrock layer (outcrop) and the amplified (peak) ground position, considering the site response characteristics, were predetermined. However, geostatistical modeling for building geotechnical spatial grids is uncertain because of the spatial density and interpolation performance of self-covariance (or variogram models). Moreover, the geodata used to determine the site response parameters vary depending on the attainability, spatial/stochastic

density for deriving geodata correlations, target area range, and priority of site classification models [18–20], and are generally categorized into two methodologies.

Proxy-based site response parameters based on terrain (elevation and slope) or geological characteristics are generally determined in large areas (e.g., nationwide) and mountainous regions with low density or high prediction errors using geostatistical cross-validation of geological survey datasets (i.e., boring-log, SPT-log, and V_S-log). The V_{SZ}-based site response parameters are typically determined when geotechnical survey datasets with the closest cross-correlations of strata-log or V_S-log along the depth are densely distributed in a narrow region (e.g., urban and infrastructure sites).

The criteria for distinguishing the two methods of site response parameters were (1) the number of boring logs in a unit grid (ea/km^2) based on kernel spatial density and (2) the standardized error in a unit grid (%) based on geostatistical cross-validation. Two methods were determined using a yes/no question regarding the criteria (Figure 1). Therefore, the site response parameters were computed as geotechnical spatial grid information, assembled with the site class and amplification factor to empirically calibrate the time-domain parameters of ground motions, such as the peak ground acceleration (PGA), peak ground velocity (PGV), and peak ground displacement (PGD) measured from the bedrock.

To evaluate site-specific landslide hazards during earthquakes for macrozonations in South Korea (with a unit area greater than 4 km^2), a digital terrain model was typically used as the backbone dataset [21,22]. In the second phase, to evaluate seismic-triggering landslides using the spatial grid, the displacement associated with the peak ground acceleration was estimated simultaneously with the dynamic safety factor using an amplification factor based on the friction, cohesive strength, and thickness of the soil layer. However, building areas require a subdivision of the spatial grid to evaluate spatial differences in seismic performance at the building basement. In the third phase, structural failure owing to earthquake occurrence was evaluated based on a seismic fragility curve. The fragility curve of a structure represents the excess probability of a specified damage level at a specific earthquake intensity. The correlated peak ground acceleration was used as the intensity index for the fragility functions, and the failure probabilities were calculated. The damage grades of the superstructures were determined based on the probability of failure. The results of the three stages of analysis were assembled into a grid in batches and evaluated independently of the type and level of seismic hazard. Each step was visualized as a map, and a confidence level was assigned to each grid unit based on the accuracy of the empirical correlations and the geospatial model.

2.2. Site-Specific Evaluation of Seismic Site Effect

The first phase was defined as the geotechnical spatial grid construction using the geostatistical method (Figure 2). In this procedure, prerequisite information related to geotechnical zonation was input into a geotechnical spatial grid, which was then used as primary data to determine the subsurface characteristics that were correlated with the seismic response that caused landslides and structural failures. To build a reliable spatial grid for the current ground conditions of the target site, it is necessary to consider both geographic conditions and geotechnical dynamic properties from site investigation reports. To build up the spatial grid, the geodata were composed of a suitable proxy (slope, elevation, landform), geotechnical data (geolayer, SPT-N, V_S, soil properties), structural data, and seismic monitoring data. When an earthquake strikes a target site, rock accelerations are recorded by the accelerometers and transmitted in real time to a spatial grid assigned with V_{SZ}- and proxy-based site response parameters. Subsequently, the seismic amplification factors are determined simultaneously at each spatial grid assembled with the site response, parameter-based site class.

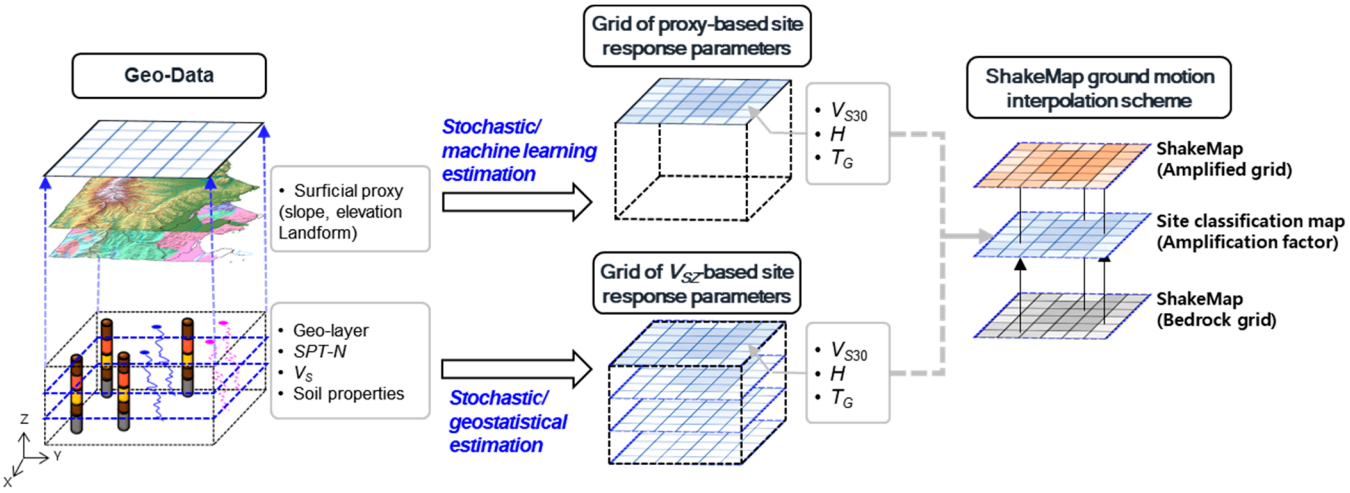


Figure 2. Schema of geodata for seismic site effect estimation and conceptual procedure of seismic amplification characterization based on geotechnical grid information.

Geostatistical methods are required to understand local ground conditions because there are spatial constraints on collected borehole data, which only provides a 1D profile in 3D space with a limited amount of data over a large target area [23]. Thus, the 3D kriging technique was applied to the extended area to estimate the spatial distribution of multi-geotechnical profiles with depth using the Unified Soil Classification System (USCS)-based geolayers and engineering parameters (e.g., V_S) correlated within SPT-*N*. Consequently, the engineering soil profile was interpolated with a 3D spatial geometry that represented each soil stratum (fill, alluvial, and weathered residual soils). Based on the 3D primary soil profile, a specific soil profile, classified by the USCS and V_S, was interpolated using 3D kriging [24].

The seismic response assessment of site-specific ground motion amplification for large metropolitan areas has been conducted by applying GIS-based data preprocessing and geographic spatial analysis, rather than instrumental or numerical site response analysis [25,26]. A site classification system quantifies and differentiates local seismic site effects based on the nonlinearity of the site response characteristics [17]. In the site classification system, the geotechnical site response parameters related to the subsurface characteristics were used as the classification criteria. The Korean and global standards for site classification systems recommend V_{S30}, which is the average V_S up to 30 m below the ground level, and $V_{S,Soil}$, which is the average V_S along the soil layer [17]. In contrast, the bedrock depth (H), which has been considered a simple empirical indicator, only reflects the geometric distribution of the site without considering the geotechnical stiffness, V_S. In addition, the ground type, stratigraphy, thickness, stiffness, average shear wave velocity (V_{SZ}), and site natural period (T_G) of the upper soil layer on the bedrock were used as the main parameters for site classification [27]. Sun et al. [24] proposed local correlations based on the type of geolayer and its soil materials between V_S and SPT-*N* values by statistical regression analysis using coupled SPT and V_S logging measured by downhole tests of surface wave methods. Because there are numerous SPT-*N* profiles, the correlated 1D V_S profiles with geolayers were archived to compute the geotechnical site response parameters. In this study, 2.5D-geometry (Figure 2), by overlaying the 2D spatial grid assigned with geolayers and V_S value depthwise (at 1 m interval), was configured based on the geosatistical modeling framework (composed of spatial density analysis and interpolation) proposed by Sun and Kim [17].

Because the existing general geospatial information predicts the stratigraphic information of the entire region, only the geotechnical survey data are secured within the target area, and errors in the predicted stratigraphic information occur where data are scarce. In particular, at the boundary of the target area or in mountainous or hilly areas where data are relatively scarce, rock may be predicted as soil, resulting in errors in evaluating

site-specific seismic response characteristics [28,29]. To reduce such spatial prediction errors and predict reliable regional seismic responses, a method for constructing a proxy-based geotechnical spatial grid assigned thematic coverage information, and overlaid with various layers as the top layer of the spatial grid, such as digital elevation model (DEM), geological maps, land cover, and satellite imagery, was developed. A DEM with 5 × 5 m resolution (0.15 arcsec) was used in combination with interferometry to gather topographic (elevation) data corresponding to the mountainous regions and, obtained from NASA's Shuttle Radar Topography Mission (http://www2.jpl.nasa.gov/srtm/instr.htm, accessed on 22 January 2024) and other local radar-mission projects to render the surficial terrain information concerning the region of interest.

Kim et al. [30] developed a data-driven workflow for obtaining principal features related with site response parameters from DEM according to the following procedures: (1) topographic position index (TPI)-based landform classification; (2) geostatistical interpolation for building a geospatial grid with geotechnical and DTM features; (3) calculation of V_{S30} grids; (4) reclassification and subgrouping of the TPI-based landform class with respect to V_{S30} grids; and (5) uncertainty analysis with regression modes, landform class, and N-V_S correlation. In this study, a 2D grid of proxy-based site response parameters (Figure 2) was constructed using a machine learning-based multivariate regression model based on terrain-based features (elevation, slope, and TPI) [30].

The seismic design standards present a site classification system for predicting ground motions during an earthquake, and thus seismic disaster prediction, as well as more systematically determining the design ground motions by considering seismic site effects. These site classification systems serve as fundamental indicators not only for seismic design, but also for early warning and rapid response to reduce earthquake damage. Site classification systems that reflect local site response characteristics have been rationalized in both South Korea and abroad [9,31,32]. In this study, a site classification system (Table 1) was introduced for domestic regions and applied as the foundation for providing regional seismic utilization information. The ground motion can be determined for seismic design by site classification using seismic response parameters and calculating the short-period site amplification factor (F_a) as well as medium- and long-period site amplification factors (F_v) [17].

Table 1. Site classification system using both V_{S30}, H, and T_G in South Korea (modified from Kim et al. [20,30].

Generic Description	Site Class		V_{SZ}-Based Criteria			Proxy-Based Criteria			Amplification Factor	
			H (m)	V_{S30} (m/s)	T_G (s)	f_0 (Hz)	Slope (%)	Elevation (m)	F_a	F_v
Rock	B		<6	>760	<0.06	>16.67	>5.6	>80	1	1
Weathered rock and very stiff soil	C	C1	<10	>620	<0.10	>10.00	>3.5	>60	1.28	1.04
		C2	<14	>520	<0.14	>7.14	>2.0	>45	1.45	1.09
Intermediate stiff soil		C3	<20	>440	<0.20	>5.00	>1.1	>31	1.65	1.13
		C4	<29	>360	<0.29	>3.45	>0.62	>22	1.9	1.19
Deep stiff soil	D	D1	<38	>320	<0.38	>2.63	>0.23	>18	2.08	1.23
		D2	<46	>280	<0.46	>2.17	>0.08	>14	2.26	1.29
		D3	<54	>240	<0.54	>1.85	>0.023	>11	2.48	1.36
		D4	<62	>180	<0.62	>1.61	>0/006	>9	2.86	1.43
Deep soft soil	E		≥62	≤180	≥0.62	≤1.61	≤0.006	≤9	1.50	1.5

V_S topographical computations have shown positive correlations with DEMs, geological maps, and other geomorphic markers [33]. The scientific notion of a terrain proxy criterion was developed for a metropolitan area in South Korea that included mountains, valleys, plains, and locations with a variety of geological features [30]. In South Korea, empirical correlations between site response characteristics and site-specific geospatial factors have been proposed for the regional zoning of seismic site effects (Table 1). As V_{S30} decreased, the strata rigidity weakened, and the height and slope decreased. Consequently, grids assembled with site amplification factors (Table 1) calibrate the recorded PGA and are now referred to as the amplified grid (i.e., ShakeMap).

2.3. Mapping of Earthquake-Induced Landslide Hazard

To evaluate site-specific landslide hazards during earthquakes for macrozonations in Korea (with a unit area more than 4 km^2), grid-based mapping for earthquake-induced landslide hazard assessment based on an amplified spatial grid and DEM-based slope of geodata is proposed [21]. Landslide hazards during earthquakes can be estimated through the dynamic factor of safety and Newmark displacement-derived horizontal amplification factors for flexible slopes with inclined bedrock, in conjunction with the characteristic values (e.g., soil thickness, shear strength, slope) of a geotechnical spatial grid. To evaluate the seismic stability of a landslide, the pseudo-static and the Newmark's sliding block methods are frequently used concurrently. Both methods assume that the target area has an infinite slope. Since the Newmark method assumes the active block as a rigid body, it cannot consider the attenuation effect of seismic waves within the block and cannot consider the change in the strength parameters with depth. Thus, there are limitations of analyzing the critical (yield) acceleration for seismic stability of slopes as a constant. However, it is known that it can predict the displacement of slopes during earthquakes relatively well based on verification by comparing it with the landslide inventory. The Newmark sliding block method [34] is adopted in NAVFAC-DM-7.1 [35], a design manual of the Naval Facilities Engineering Systems Command.

The maximum displacement (d_{max}) per unit grid of geotechnical spatial grid is expressed as follows:

$$d_{max} = \frac{V_{max}^2}{2a_c} \cdot \frac{a_{max}}{a_c} \quad (1)$$

where a_{max} is the peak ground acceleration, a_c is the critical acceleration, and V_{max} is the maximum velocity. a_c is calculated based on the factor of safety given under static conditions (FS_{static}). If the slope has a complex geometry or is reinforced, it can be obtained by pseudo-static method analysis, and the seismic coefficient at a FS_{static} of 1 can be defined as a_c [34]. In this study, a_c is computed by $(FS_{static} - 1)\sin\alpha$, where α is slope angle (°) determined from the DEM. To compute the FS_{static} within the geotechnical spatial grid (Figure 2), a relatively simple limit-equilibrium model of an infinite slope in material which has both internal friction angles (ϕ), cohesion (c), degree of saturation (S), unit weight of water (γ_w), total unit weight of soil (γ_t), and soil thickness (h) can be used. The FS_{static} is as follows:

$$FS_{static} = \frac{c}{\gamma_t \cdot h \cdot \sin\alpha} + \left(1 - \frac{S \cdot \gamma_\omega}{\gamma_t}\right) \frac{\tan\phi}{\tan\alpha} \quad (2)$$

ϕ, c, and γ_t per unit grid are determined by the geotechnical spatial grid having measured properties by in situ/laboratory experiments or the empirical correlation between SPT-N value and ϕ (i.e., $\phi = \sqrt{12N} + 15$), and c ($c = N/0.144$) [35]. h is determined as the sum of the thickness of the geolayer based on the geotechnical spatial grid. The saturation of the soil layer is assumed to be 100% for a conservative assessment, assuming that earthquake and rainfall occur simultaneously. For the FS_{static} for the slope, it was assumed that the groundwater level in a fully saturated slope coincides with the ground surface (i.e., $S = 1$). However, there are uncertainties of the dynamic factor of safety and Newmark displacement due to the site-specific determination of the shear strength constants and saturation as follows:

1. The uncertainty of the transformation method between SPT-N value and ϕ, and c.
2. The uncertainty of SPT-N value, based on the geotechnical spatial grid.

Although the dynamic factor of safety decreases as the saturation of the ground increases or the adhesion decreases [34,35], the uncertainty analysis should be performed in further study.

In this study, the dynamic safety factor ($FS_{dynamic}$) for slope failure is calculated for each grid square as follows:

$$FS_{dynamic} = \frac{c + (\gamma_t + S \cdot \gamma_w) \cdot h \cdot cos\alpha \cdot tan\phi}{\gamma_t \cdot h \cdot sin\alpha + k_\alpha \cdot \gamma_t \cdot h} \quad (3)$$

where k_α is the seismic coefficient, assumed to be the seismic acceleration divided by the gravitational acceleration. In this study, $FS_{dynamic}$ was denoted as FS. The severity of the dynamic factor of safety was categorized into three levels ('High', 'Moderate', 'Low') for $0 < FS \leq 1.1$, $1.1 < FS \leq 2.0$, and $FS \geq 2.0$. In the slope design standards in South Korea, the reference safety factor applied to the static stability of slopes is 1.1, and the reference safety factor applied to seismic design for stability analysis during earthquakes is also 1.1. According to relations between FS and manifestation induced by landslides, areas determined as $FS < 2.0$ were identified by extensive lateral spreading. Thus, the threshold of FS was assumed as three class based on the local design standards and manifestations, however, the uncertainty due to the criteria of FS should be validated in further study.

The pseudo-static method for seismic slope stability is based on the assumption of limit equilibrium and remains the most widely used method in geotechnical engineering practice. Pseudo-static analysis provides an index of stability (FS), but there is no information concerning the deformations associated with slope failure. Because the serviceability of a slope after an earthquake is controlled by deformations, analyses that predict slope displacements provide a more useful indication of seismic slope stability [3]. Newmark's method was used to calculate the cumulative displacement of a landslide as a rigid plastic block sliding on an inclined plane. The block had a known a_c, which was simply the threshold base acceleration required to overcome the shear resistance and initiate sliding. The analysis calculated the cumulative permanent displacement of the block relative to its base as it was subjected to an earthquake acceleration $a(t)$. The cumulative displacement was calculated by double integrating the area under the accelerogram that exceeded the critical acceleration. However, several simplified approaches for estimating the Newmark displacement have been suggested empirically by several researchers because Newmark analysis is time-consuming and performing double integration is notably difficult [36,37]. In this study, the models of Ambraseys and Menu [37] were also used as follows:

$$log(D_N) = 0.9 + log\left[\left(1 - \frac{a_c/g}{a_{max}/g}\right)^{2.53}\left(\frac{a_c/g}{a_{max}/g}\right)^{-1.09}\right] \quad (4)$$

where D_N is Newmark displacement (cm). Based on the dynamic displacement hazard classification of the United States Geological Survey (USGS), the severity level was divided into four levels: Low (<10 mm), Moderate (10–50 mm), High (50–150 mm), and Very High (>150 mm) [37].

2.4. Seismic Impact Analysis Based on Structure Fragility

The fragility of a structure or component is defined as the conditional frequency of failure given the response parameter value. The response parameter x could be the force on the component or structure induced by wind, stress owing to an earthquake, etc. The conditional frequency of failure F_0 given x_0 represents the fragility of the component at that level. In other words, the fragility curve represents the cumulative distribution function of the capacity of the component to withstand imposed stress x. In several seismic risk studies, the response parameter x is the peak horizontal ground acceleration, measured in units of g, and the gravitational acceleration. Furthermore, the fragility curve is typically a

lognormal distribution (other distributions have also been considered, such as truncated lognormal and normal distributions).

The time-variant reliability problem, in broader terms, is the problem of calculating the probability that a nonlinear system with random properties exposed to random, time-varying actions will cease to satisfy a number of requirements, the definition of which is also uncertain. For seismic reliability, it is common to obtain the abovementioned probability conditionally on an intensity measure of the input ground motion, known as the fragility function. To compute the unconditional probability at a given site and in a given period, the structure fails to perform satisfactorily, and the uncertainty in the seismic intensity is reintroduced using the hazard function (complementary cumulative distribution function (CDF) of the intensity) by convolving the derivative of the latter with the fragility function, resulting in what is commonly referred to as seismic risk.

In the past two decades, a large number of methods for computing fragility functions have been proposed, ranging from expert judgment to data analysis on observed damages [38,39], to fully analytical approaches, as observed in Cornell et al. [39]; Gardoni et al. [40]; Au and Beck [41]; Schotanus et al. [42]; and Lupoi et al. [43]. General reviews are available in Kiureghian [44] and Pinto et al. [45]. A common feature of most analytical approaches is the use of a reduced number of simulations to probabilistically compare the maximum structural responses with the corresponding capacities. The primary difference between them is their balance between cost and accuracy, that is, their ability to economically account for all aspects of the reliability problem. These latter include:

1. The possibility of a structure collapsing in more than one failure mode (system reliability problem), which is common for civil engineering structures such as multistory buildings and bridges.
2. Interdependence of failure modes.
3. Uncertainty in the structure capacity owing to the approximate nature of the models and the variability of the system parameters.
4. The influence on the dynamic response of the variability of the system parameters.

The fragility function of a structure represents the excess probability of a defined damage level at a specific earthquake intensity. An intensity index, or earthquake intensity, is required to represent the damage probability. Spectral acceleration (S_a) and spectral displacement (S_d) are commonly used intensity indices based on structural characteristics. It is convenient to calculate the damage probability of a structure instantaneously using peak ground acceleration (PGA) as the intensity index.

Damage probability of the superstructure is expressed as follows:

$$PF_{ij} = PROB[D \geq C_i | EQ_j] \tag{5}$$

where PF_{ij} denotes the probability of exceeding i level for an earthquake with an intensity of j, D denotes the effect of the load by an earthquake, and C_i denotes the strength of the structure at damage level i.

Indices that properly represent structural damage should be selected. Fragility is a cumulative lognormal distribution function that is normally expressed as follows:

$$P_f(s) = \phi\left[\frac{\ln s - \ln \bar{s}}{\beta}\right] \tag{6}$$

where $P_f(s)$ denotes the damage probability of structure at s, $\phi[]$ denotes a Gaussian cumulative lognormal distribution function, $\bar{s}$ denotes the median of PGA at ground surface, s denotes the PGA of the earthquake, random variable, and β denotes the standard deviation of the log value of the PGA at ground surface.

To evaluate structural susceptibility in real time, the fragility function was used as the threshold of structural failure and linked with a geotechnical spatial grid (assigned correlation equations for seismic load determination). Superstructures for seismic fragility evaluation are divided into two groups: structures above the soil layer and structures above

the rock (Figure 3). The fragility of the structure above the soil layer is evaluated based on the peak ground acceleration linked with the seismic load correlation to consider the site-specific response characteristics. The fragility of the structure above the rock, where a seismic wave passes directly, is evaluated in relation to the rock outcrop acceleration transmitted by the accelerometer.

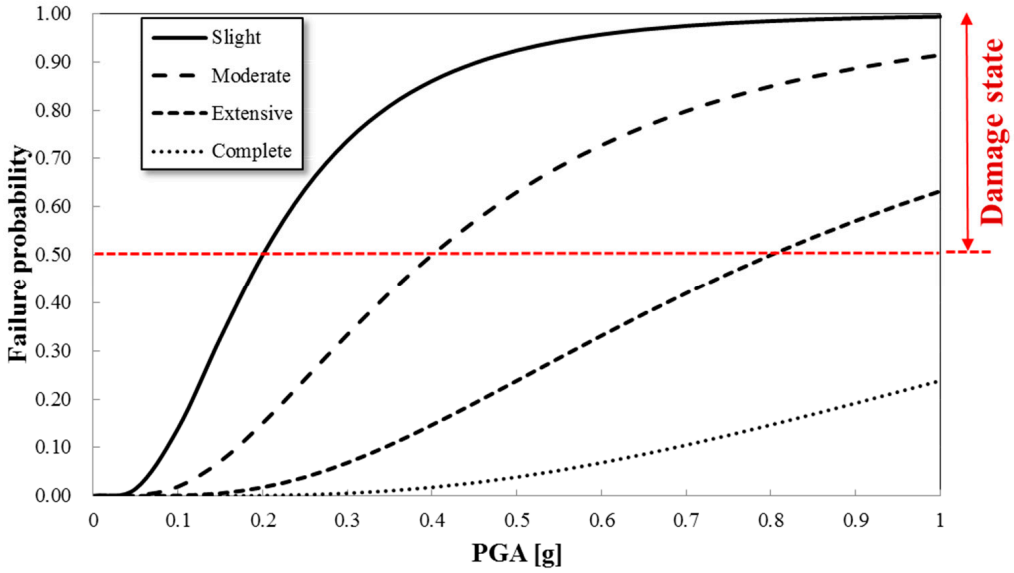


Figure 3. An example of fragility curve and damage state for unreinforced concrete structure modified from Kim and Chung [21].

The damage level of a structure during an earthquake is represented by the probability of failure using the fragility function. In this study, the method determining damage grade was determined using the probability of failure at each damage level to estimate seismic damage to structures. First, the failure probability of each structure is calculated using either the transmitted rock outcrop acceleration from the accelerometer or the correlated PGA based on the statistical correlation for the seismic load.

Second, the seismic damage probability ($P_f(a)$) with a geotechnical spatial grid was determined by transmitting a_{rock} or PGA in the seismic fragility function. It was assumed that a damage grade would be assigned when the probability of each damage level exceeded 50%. The most severe damage grade among the probable damage grades of the target structure was determined as its grade. For example, in the case of a concrete frame, if the probabilities of 'Slight' and 'Moderate' levels are both greater than 50%, then the damage grade of the structure is confirmed as 'Moderate' (Figure 4). Third, the structural damage state (or class) for the target structure was evaluated by considering the occupied area ratio of the geotechnical spatial grids with $P_f(a)$ values. If the occupied area ratio of $P_f(a)$, determined as the damage state (e.g., Slight, Moderate, etc.), was more than 50%, the structural damage state of the target structure was 'Failure', corresponding to the damage level.

3. Verification of Framework Using Observed Inventory from 2017 Pohang Earthquake

3.1. 2017 Pohang Earthquake-Triggerd Damage Inventory

For the quantitative predictive evaluation of geotechnical hazards caused by the 2017 Pohang Earthquake, an optimal evaluation scheme suitable for reliable spatial zoning of geotechnical and seismic engineering was validated using an actual damage inventory. The 2017 Pohang earthquake (M_W 5.4) was South Korea's second most significant seismic event in recent decades, causing the most structural damage and injuries [7]. The extent of damage from ground motion amplification and liquefaction was exacerbated because the earthquake epicenters were located in areas with thick quaternary sediments and alluvial deposits [46].

Given the challenges involved in compiling a comprehensive earthquake damage inventory for the Pohang area, it is crucial to evaluate regional seismic site effects and their associated impacts, including observable land deformations and structural failures. To ensure the prediction accuracy of the proposed framework, the trigger analyses and severity criteria were verified by comparing them to manifestations or damage inventory observed during the 2017 Pohang earthquake prior to developing a seismic hazard map.

According to a geological map with lithofacies, geological boundaries, and fault information from the Korea Institute of Geoscience and Mineral Resources, the Pohang Basin is composed of Miocene (~20 million years ago) non-marine to deep marine sedimentary strata with bedrock [17] (Figure 4). Soil development in the Gokgang River Basin is primarily because of fluvial processes and is spatially categorized as quaternary alluvium. These zones of thick soil and deep bedrock are vulnerable to ground motion amplification during earthquakes owing to site effects [10].

A post-earthquake assessment was conducted four days after the mainshock to quantify earthquake damage in accordance with established field guidelines [47]. Owing to variability in surveyor sensitivity, establishing clear guidelines for damage quantification is difficult, though indicators to represent damage severity have been defined. The assessment classified geotechnical hazards into ten grades based on site morphology and soil stability, and structural damage was categorized into ten grades based on crack type and failure mode (hollow circles in Figure 4). Key information from the field assessment, including peak ground acceleration (PGA), site class, and hazard grades, was reported for each damaged building, and the damage was categorized into five states: 'Safe', 'Slight', 'Moderate', 'Extensive', and 'Complete'. The majority of the damage was concentrated within 5 km of the epicenter; however, the effects of liquefaction and subsidence were not fully addressed. Specifically, structures classified as more severe hazard grade (>6) were located near the epicenter (approximately 2 km).

Because the post-earthquake survey was performed in an urban area, macroscale land deformation in the mountainous area was archived to detect the occurrence of landslides. The land creep area, where the landslide monitoring station was installed, was obtained from the Korea Forest Service [48] (black points in Figure 4). InSAR-based displacement across the entire center of Pohang City was also reported by Fadhillah and Lee [49]. The Pohang earthquake provides a unique opportunity to refine Korea's static slip model, owing to its shallow focal depth (~4 km) and successful acquisition of surface displacement data from Sentinel satellites. A linear slip inversion of the InSAR data revealed that significant slip occurred in the northeastern region of the hypocenter, with a rupture measuring 5 km in width and 6 km in length and a mean slip of 15 cm. The target area's maximum surface displacement was reported to be 6 cm, with the majority concentrated northeast of the epicenter.

3.2. Verification of Amplified ShakeMap

The site class was based on the modeling procedure of the geotechnical spatial grid (Figure 1). Borehole datasets were used for seismic hazard mapping (Figure 5a). Estimates of the geotechnical layers were acquired from approximately 1913 existing borehole datasets (Figure 5a). The study area was divided into 100-m mesh areas, yielding 1512 grid squares. Component mesh unit datasets were generated for each grid square [7]. Seismic zones were defined by classifying sites and calculating site coefficients using a system that incorporated geotechnical criteria (Table 1). The study area featured a maximum bedrock depth of approximately 28 m, with bedrock at a depth of approximately 20 m, mainly found in the central plain (Heunghae Basin) and the coastal reclaimed downtown (Jangseong-dong). In coastal plain areas with dense residential and industrial facilities, V_{S30} values ranged between 320 and 520 m/s (Figure 5b).

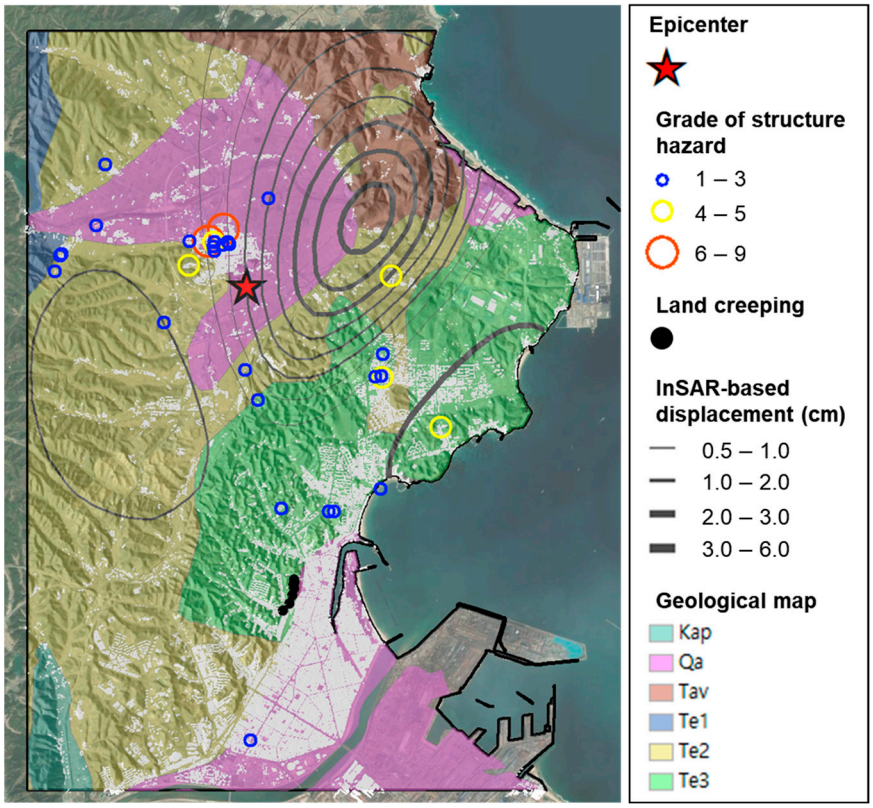


Figure 4. Epicenter of 2017 Pohang earthquake and spatial distribution of triggered damage inventory (defined as grade of structure hazard), reported by Kim et al. [7], around the epicenter (i.e., target site). Areas of land creeping, reported by Korea Forest Service, and InSAR-based displacement, reported by Fadhillah and Lee [49], are also indicated. The base-map is a geological map.

To investigate the earthquake damage, a framework for assessing seismic site effects was developed and applied to the epicenter of the Pohang earthquake [7]. This study discovered that ground motion amplification varied with site conditions, with higher earthquake intensities being associated with lower amplification. An analysis of building damage in areas with approximately 35 m of alluvial sediment revealed that buildings on softer sites (site class C2–D1) [17] were more severely damaged [7]. Low-rise buildings (2–4 stories) with minor to moderate damage were primarily located at softer sites. This study also correlated building damage with seismic site classifications and severity categories, indicating that amplified ground motions caused more liquefaction-related damage. This leads to a more severe site response/deformation and induces building failures.

To understand the peak ground acceleration (PGA) incorporated with the site amplification factor of the geotechnical spatial grid, ShakeMap (Figure 5c) [50], computed using free-field acceleration at the rock outcrop, was used (Figure 5c). Grids with a higher PGA (>0.3 g) were densely distributed in the northeast region of the epicenter, where the InSAR-based displacement was measured up to 6 cm. The amplified grids with PGA over 0.35 g accounted for 75% of land displacement areas over 2 cm observed from the InSAR processing. The amplified grid (i.e., the amplified PGA above the surface) was determined by calibrating the recorded PGA based on the assembly with F_a. Consequently, the ShakeMap based on the amplified grid was characterized to range from approximately 0.09 g to 0.48 g. The spatial heterogeneity of the PGA varied and was biased along the Heunghae Basin when compared to the recorded ShakeMap. The grids were used to identify the potential severe seismic zone using geotechnical grid-based landslide and structural fragility analyses.

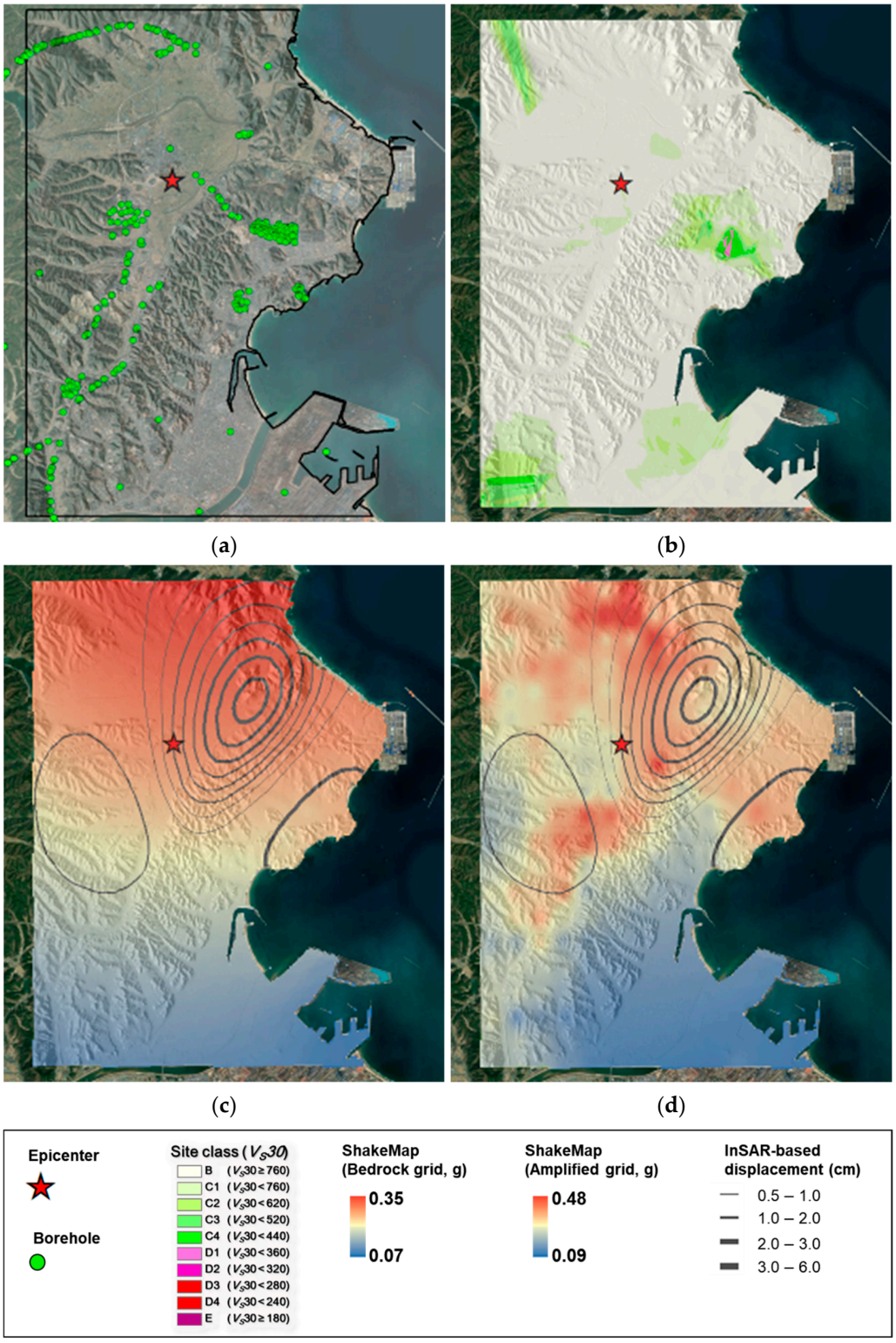


Figure 5. Grid information at the target site to assess the site-specific seismic site effect: (**a**) spatial distribution of borehole datasets in geodata; (**b**) ordinary kriging-based geospatial grid information of V_{S30}; (**c**) measured ShakeMap during mainshock of 2017 Pohang earthquake; and (**d**) amplified ShakeMap applying the amplification factor assigned at grid information (**b**).

3.3. Verification of Landslide Hazard Map

The safety factors for static and seismic slope stability were calculated using the amplified grid (Figure 5d), slope DEM, soil depth, and internal friction angle information.

Figure 6 shows the landslide hazard map at the target site using the dynamic factor of safety and Newmark displacement against the 2017 Pohang earthquake, based on the amplified grid (ShakeMap) assigned to the amplification factors (Figure 5b). A factor of safety lower than one ('High' level) is not common for the target area in Pohang city (Figure 6a). The area with a distribution of a dynamic factor of safety less than one increases as the PGA of the amplified grids (Figure 5d) increases, but only for mountainous regions. In addition, the area with a distribution of a dynamic factor of safety higher than two decreased as the PGA increased. The center points of the observed landslide manifestation (land creeping), presented as a blue dot circle (Figure 6), were spatially assigned to the grid of dynamic factor of safety and Newmark displacement. The 90% grids of land creeping (about 65 mm-lateral displacement) were overlaid on the grid of $0 < FS \leq 1.1$ ('High' level).

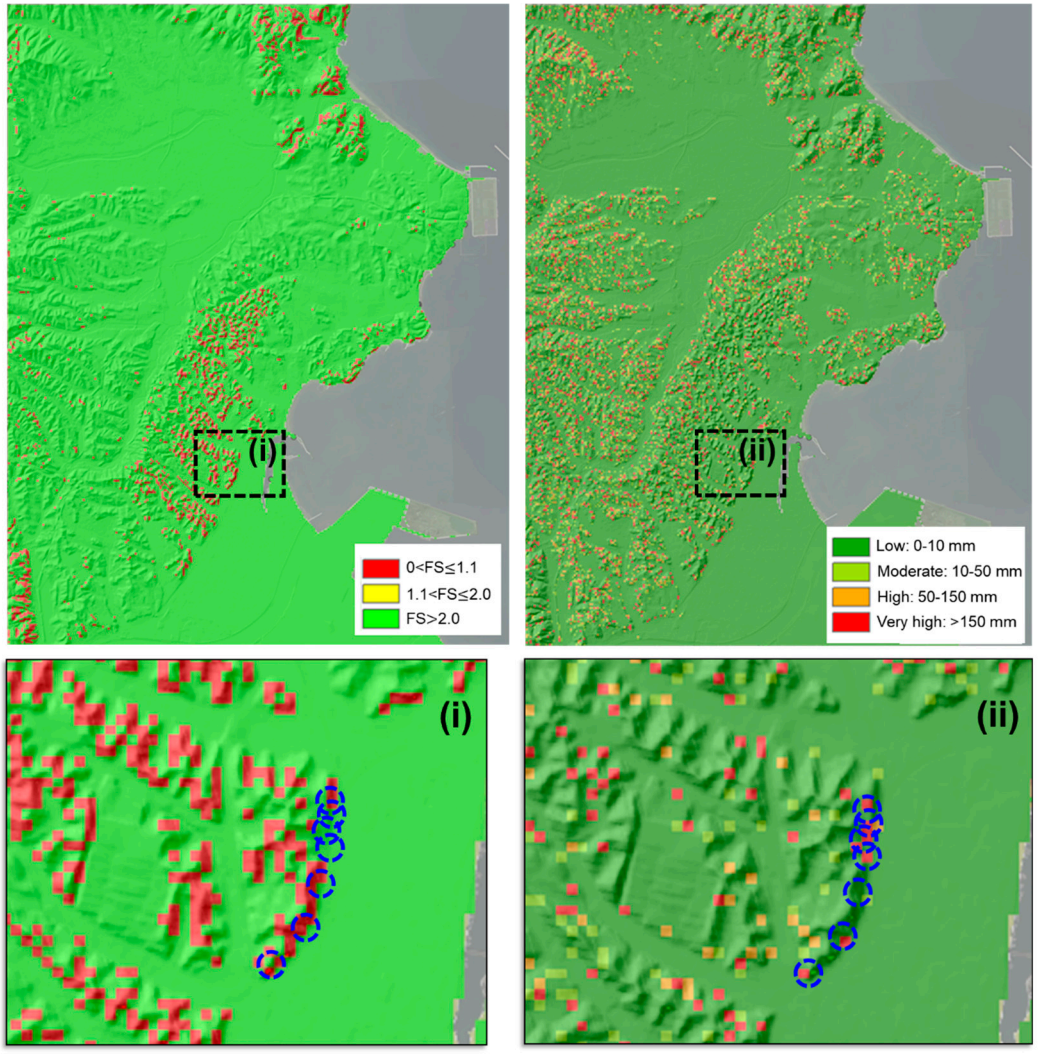


Figure 6. Landslide hazard map at the target site by (**a**) dynamic factor of safety, and (**b**) Newmark displacement against 2017 Pohang earthquake based on the amplified grid (ShakeMap) assigned with the amplification factors (Figure 5b). The area of observed landslide manifestation (land creeping), 65 mm displacement, are also presented as blue dot circle.

Figure 6b shows the results of the Newmark displacement during the 2017 Pohang earthquake. The yield acceleration was calculated using the dynamic factor of safety from Equation (1), while the Newmark displacement was calculated using Equation (4). Moreover, the severity class of Newmark displacement was classified into four levels ('Low',

'Moderate', 'High', 'Very high'). Consequently, a displacement of more than 99% area was produced within 10 mm because most of the factors of the safety values in each case were higher than one, as shown in Figure 6a, and many factors in Table 1 were assumed or neglected in this analysis. In contrast, the majority of steep mountainous regions with a slope over 30% (more than 65%) for the higher PGA grids (>0.35 g) were evaluated at the 'High' or 'Very high' level. Considering synthetically the dynamic factor of safety and Newmark displacement, it is possible that the mountainous regions of the target area can be damaged 'High' level (dynamic displacement: 50–150 mm) in condition of PGA greater than 0.22 g. The 80% grids of land creeping were overlaid on the grid of the 'High' or 'Very high' level.

3.4. Verification of Building Loss Map

At the target site, 65% of the residential and commercial buildings were built using unreinforced concrete methods. The fragility function of the concrete frame structure in the study area was calculated using the proposed seismic impact analysis based on structural fragility. For example, the fragility functions of concrete frames with unreinforced masonry infill walls (concrete frames) were applied based on FEMA [50]. The damage levels were arranged as 'Slight', 'Moderate', 'Extensive', and 'Complete'. Table 2 lists the median and standard deviation of the fragility functions for unreinforced concrete structures. It is assumed that seismic failure is confirmed when the probability of damage levels exceeds 50%, and the damage level and state of the concrete frame are subjected to Table 2.

Table 2. Definition of damage levels of seismic fragility curves for unreinforced concrete structure (FEMA [50]).

Damage Level	Slight	Moderate	Extensive	Complete
Mean Value ($\bar{s}$)	0.2	0.4	0.8	1.6
Standard Deviation (β)	0.64	0.67	0.66	0.66
Damage State	8%	40%	80%	100%

The fragility curve (Figure 3) was linked to the amplified ShakeMap grid (Figure 5d), which represented the site class, amplification factor, and response PGAs. Consequently, the failure probabilities for the four damage levels of the unreinforced concrete structure were calculated using amplified PGAs based on the geotechnical spatial grid. Figure 8 shows the building loss maps for each building site with respect to the four damage levels (slight, moderate, extensive, and complete) based on the fragility curve (Figure 3). A total of 85% of building sites were classified into failure states at the 'Safe' failure level ($0 < \text{Fragility} \leq 50\%$). Therefore, most target structures were regarded as safe in terms of seismic fragility, because the topsoil generally consisted of non-amplifiable boulder stones or dredged silty clay. To visually determine the detailed damage state, the target site was divided into three extended areas: earthquake disaster areas (Heunghae-Uep) (Figure 7(i)), where many major manifestations were observed; Jangsung-Dong, where failures of nonstructural components were observed (Figure 7(ii)); and downtown, where no earthquake manifestations were reported (Figure 7(iii)).

The building loss map was also compared to the kernel density of damaged buildings. At Heunghae-Uep (Figure 7(i)), 92% of buildings with a potential failure probability for seismic fragility ('Slight, 'Moderate, 'Extensive' levels) were located in the 5 ea/km^2 zone based on the kernel density of damaged buildings. At Jangsung-Dong, 95% of buildings predicted as having a 'Slight' damage level were distributed in the zone of 4 ea/km^2 according to the kernel density of damaged buildings. Only three buildings in the downtown area were classified as having 'Slight' damage levels, but these were not reported as significant manifestations of building damage. To compare the spatial coincidence between damaged buildings and damage levels above 'Slight', the AUC (area under the ROC (receiver operating characteristic)), was analyzed for four damage states (Figure 8). All damage states performed well (AUC > 0.5) [51], with greater sensitivity and

specificity in the following order: safe, slight, moderate, and extensive. Because 85% of the building sites classified as 'Safe" level were distributed among non-damaged building sites, the precision for predicting the 'Safe' level was highest among them.

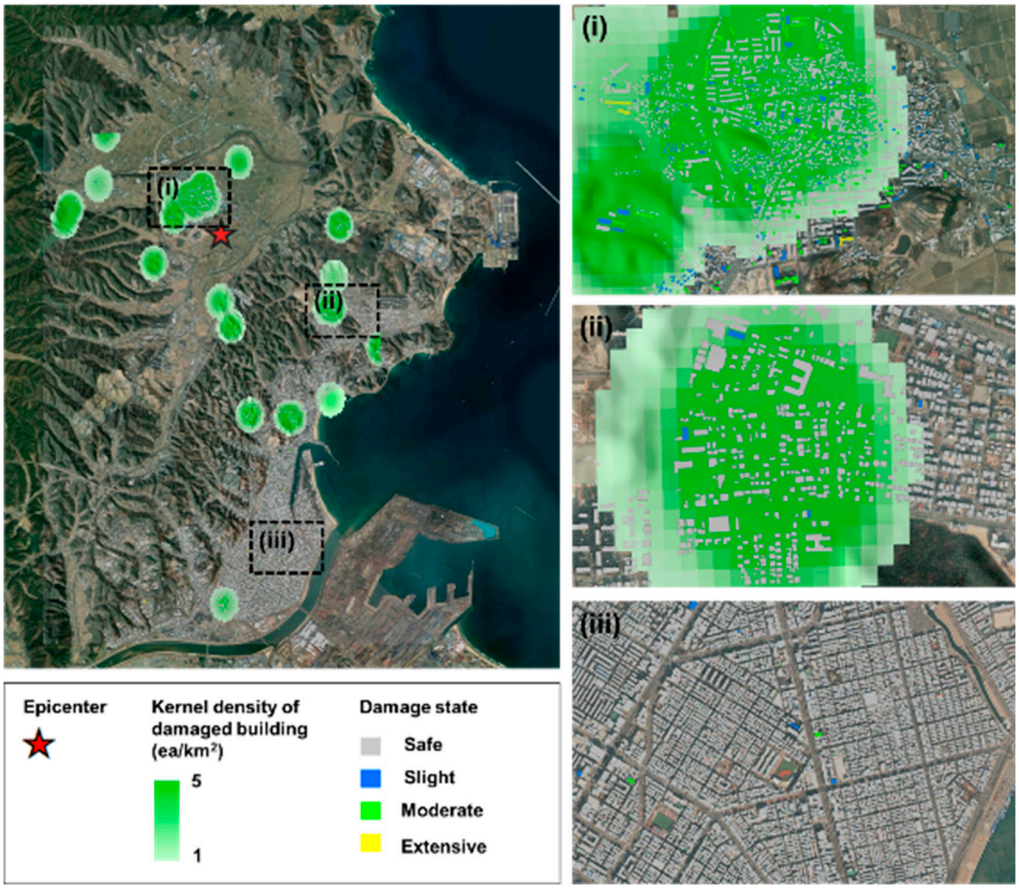


Figure 7. Building loss maps at the target site of four damage levels by slight, moderate, extensive, and complete, against 2017 Pohang earthquake based on the amplified grid (ShakeMap) assigned with amplification factors. The right pan described the three extended areas: (**i**) Heunghae-Uep, where many major manifestations were observed, and nearby epicenter; (**ii**) Jangsung-Dong, where the failures of nonstructural components were observed; and (**iii**) Downtown, where the earthquake manifestations were not reported. The kernel density of observed damaged buildings was also presented.

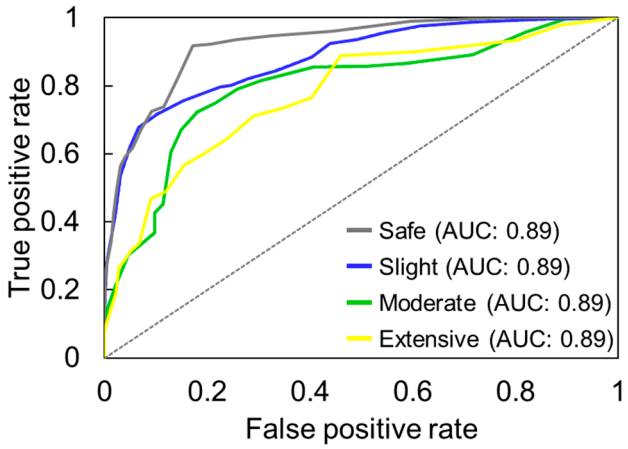


Figure 8. AUC of building loss map for four damage levels.

4. Earthquake-Induced Multi-Hazard for Gyeonggi-do Province

4.1. Site Description

In this study, comprehensive stratigraphic and geodata, such as geotechnical datasets, DEM data, building inventories, administrative district maps, and geological maps of the Gyeonggi-do region, were prioritized and collected to understand the site conditions of the entire Gyeonggi-do administrative area (Figure 9). The DEM consisted of a spatial grid network spaced 5 m apart across the administrative area of Gyeonggi-do, with a maximum elevation of 1464 m and a mean standard deviation of 6.8 m (Figure 9a). The DEM was transformed into a slope map with a maximum slope of 88.3° using an accelerated ATAN function based on the vertical to horizontal change ratio. Understanding terrain steepness is essential for tasks such as modeling erosion or assessing land stability. Geological boundary and fault line information at a scale of 1:250,000 was obtained from geological map data. In particular, 52,658 geological logs, which are required for evaluating seismic response characteristics, were obtained from 2045 construction projects (Figure 9c). To determine seismically vulnerable areas and facilities, the building register was obtained from the Gyeonggi-do government and contained detailed information such as serial management number, building name, location, number of floors, building shape (floor height, basement level), type (e.g., unreinforced masonry), seismic design, and seismic performance evaluation results (Figure 9d).

The collected geodata shared the same coordinate system (projected coordinate system: Korea 2000 Central Belt; geographic coordinate system: Korea 2000) based on the geographic information system (GIS) platform, and spatial modeling was used to analyze the geostatistical spatial analysis and seismic response characteristics. Geotechnical datasets are primarily divided into boring logs and in/ex situ soil dynamic tests of the subsurface. The boring-log data were divided into general information (e.g., drilling location/date and investigation method) and stratigraphic information, which described the characteristics of each stratum, such as thickness, color, and stiffness. It was also configured to use the Standard Penetration Test (SPT)-N and RQD values to identify the degree of weathering of the rock layers. The soil dynamic characteristics were classified as shear wave velocity by depth, resonant column test information, and repeated triaxial test information for the shear strength and damping ratio. In addition, to consider the seismic site effects owing to the topography and geological characteristics of a large area, the elevation and slope information of the DEM were linked to the geological classification and fault information of the geological map using the same spatial coordinate system.

The integrity verification of the built geodata consisted of three main steps: verification of the required field input variables, spatial coordinate information, and geotechnical outliers. To review the integrity of the collected borehole survey data, data distributed outside the target area or information with incorrect spatial coordinates were prioritized for correction and supplementation. In addition, a cross-validation-based outlier verification method [52] was used based on the depth to the bedrock, with 8.5% defined as the outlier criterion by calculating the root mean square error (RMSE) between the predicted and measured values. The RMSE of the optimized bedrock depth, after removing data that exceeded the outlier criterion, was approximately 1.8 m. The spatial correlation of the borehole survey data was relatively high, and the spatial uncertainty of the site classification was determined.

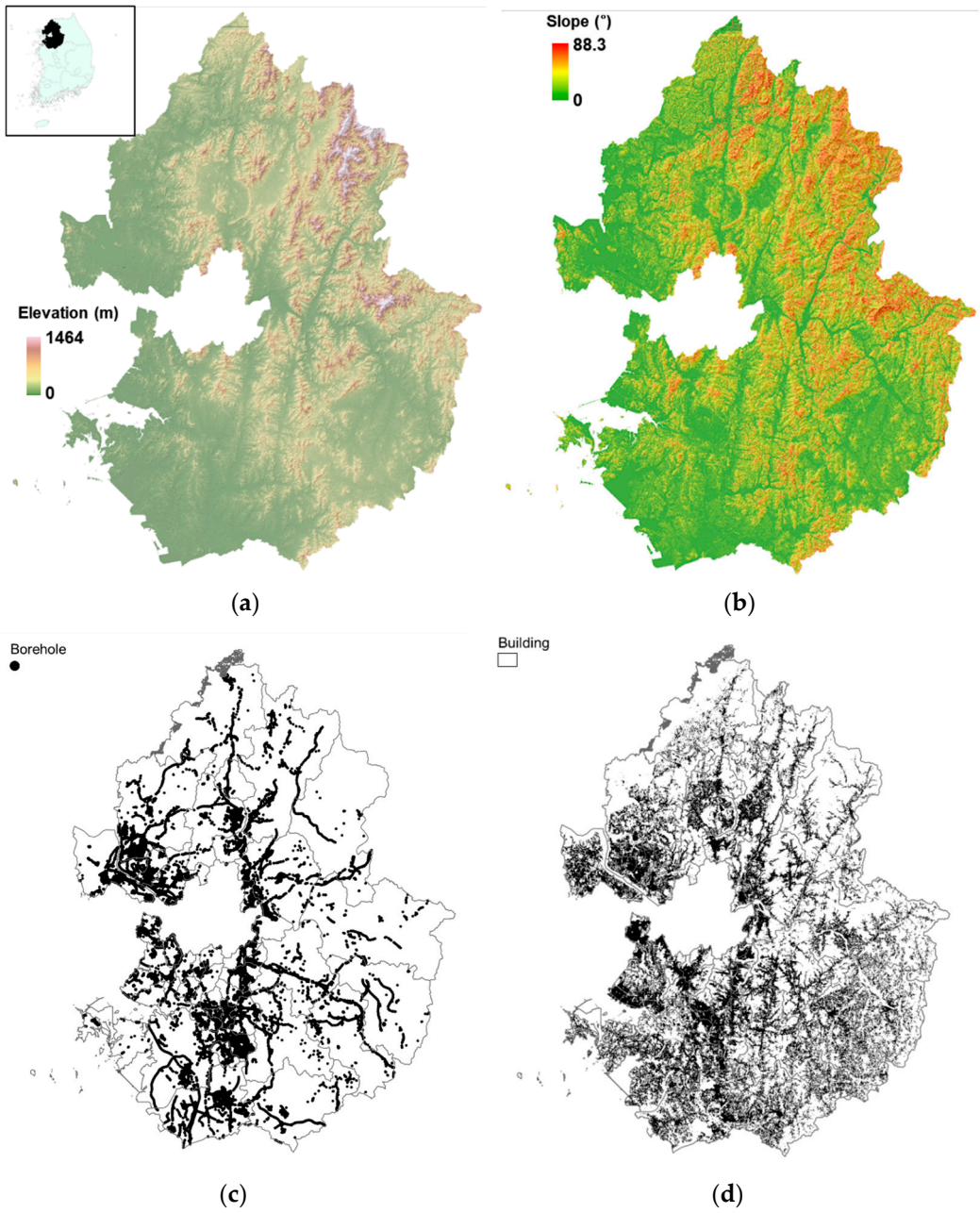


Figure 9. Collection of geodata in Gyeonggi-do area: (**a**) surficial elevation of DEM; (**b**) surficial slope of DEM; (**c**) borehole datasets; and (**d**) registered building datasets.

4.2. Geospatial Pattern Analysis Based on Geotechnical Spatial Grid

To understand the spatial distribution of site response characteristics and apply site classification using point-type boring survey data, accurate spatial distribution characteristics and spatial correlation analysis based on site-specific evaluation of seismic site effects are required. Spatial density analysis and spatial interpolation were performed using geodata from Gyeonggi-do province (Figure 10). The proposed procedure for building a 2.5D geometry was based on the geostatistical modeling framework (Figure 2), considering the spatial density analysis and interpolation. First, the number of boring logs in a unit grid (ea/km^2), based on the kernel spatial density, was computed using geotechnical spatial grids (Figure 10a). It was observed that the density was mainly high in metropolitan areas (e.g., Suwon and Ilsan) and adjacent areas centered on the periphery of Seoul by distributing 25 boreholes per unit area (100 × 100 m) from the kernel function. In the

mountainous region, 98% grids no more than 3 ea/km^2 and criteria for selecting methods of site proxy-/V_{SZ}-based site response parameters were mainly distributed.

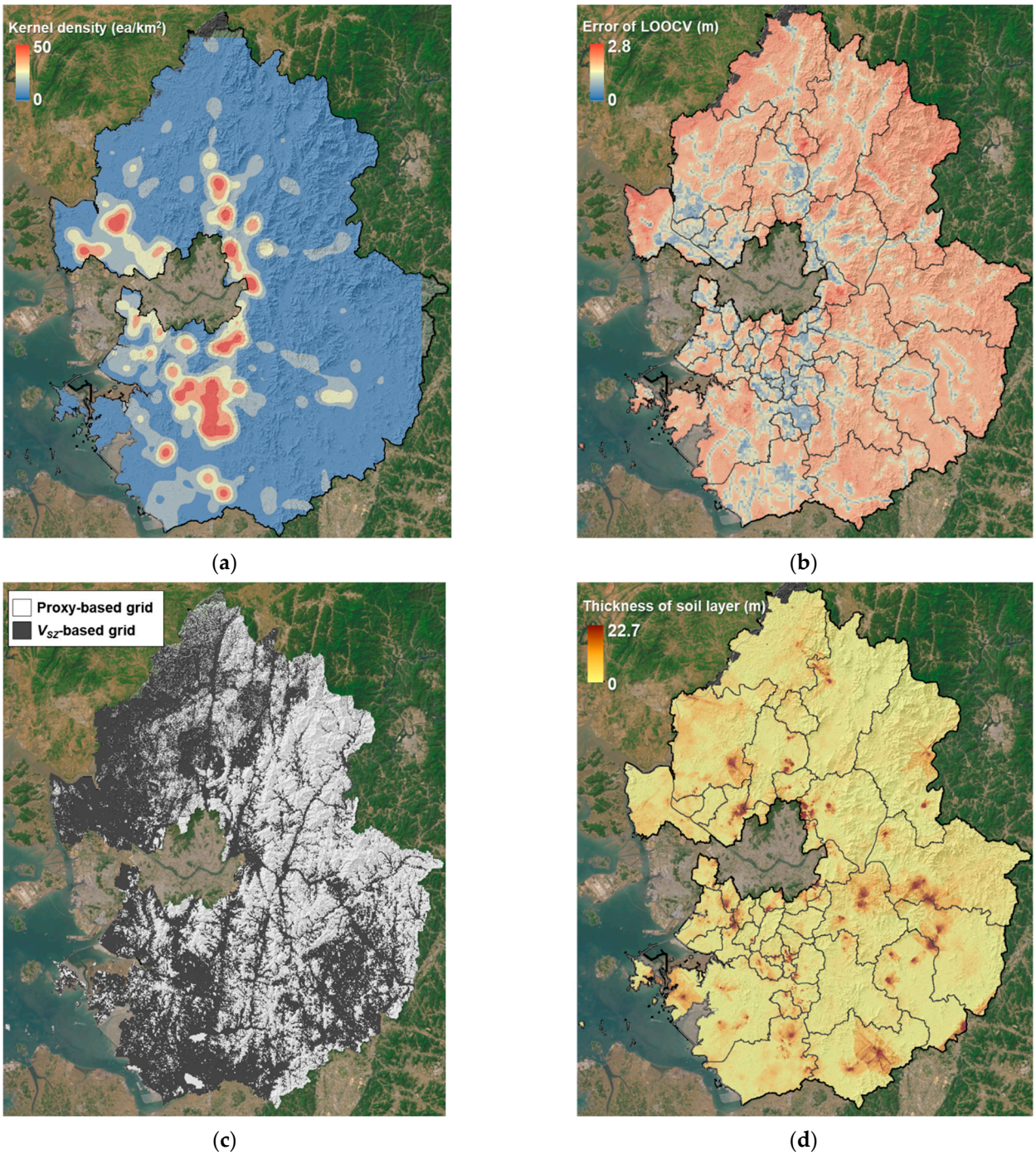


Figure 10. Geotechnical spatial grid information in Gyeonggi-do area: (**a**) kernel density of borehole datasets; (**b**) error of LOOCV by applying ordinary kriging; (**c**) composition of zones by proxy- and V_{SZ}-based site response parameters; and (**d**) thickness of soil layer.

Second, the standardized error in the unit grid (%) was estimated using geostatistical cross-validation (Figure 10b,c). Kriging is a geostatistical technique that combines mathematical and statistical approaches. In kriging, the confidence (or weight) of the existing data for a point is statistically defined as the variance. The data and predicted values are closely related to each other by the variance; thus, the farther the unknown is spatially distant from

the location of the existing data, the larger the variance of the unknown, and the smaller the weight. Sun and Kim [17] optimized spatial interpolation and site classification techniques to assess seismic site effects in the metropolitan areas of South Korea (Seoul and Busan). In this study, geostatistical spatial analysis was performed by computing the maximum value of the stratum thickness and SPT-*N* value on a spatial grid based on ordinary kriging (OK) and compared with other geostatistical techniques (e.g., simple kriging and Gaussian simulation) based on leave-one-out cross-validation (LOOCV) for the thickness of the soil layers (Figure 10b). The 80% grids had no more than a 0.1 m error of LOOCV and were distributed on the grids with no more than 3 ea/km^2 (i.e., kernel density). If a 2 m error is estimated at the grid-assigned soil layer thickness of 4 m, the 50% relative error, and a standardized error in unit grid (%) based on LOOCV, is calculated. In the mountainous regions, the average slope was approximately 30 degrees, and 70% of the grids had more than 50% relative error owing to the shallow soil layer (average thickness: 0.3 m).

Based on the two criteria (3 ea/km^2 and 50% error), two methods for developing proxy-/V_{SZ}-based site response parameters and composition zones were defined (Figure 10c). Figure 10c shows the spatial distribution of soil layer thickness in a grid with 100-m spacing using OK. The geospatial grid included a total of 1,210,194 grids. The distribution of stratigraphic thicknesses is generally concentrated in urban areas where important facilities are located. These areas have a relatively thick distribution of soil layers, centered on sites formed after the Cenozoic Era, such as alluvium and intrusive granites. In addition, the distribution of sedimentary soil layers was thicker near rivers, while that of landfill layers was thicker in urban areas. The weathered soil layer was also relatively thick near rivers and urban centers at lower elevations, indicating that the soil layer was relatively thick in low-elevation areas. This implies that seismically vulnerable soil layers are thicker in areas where the population and industry are densely concentrated, which can exacerbate damage during an earthquake. The geostatistical analysis and seismic ground response characterization results from this study were organized into fields of the corresponding geospatial grid to investigate the possibility of expanding the use of site classification for administrative and facility areas.

4.3. Seismic Site Classification and Its Amplification

The seismic response assessment of site-induced ground motion amplification in Gyeonggi-do was carried out using data processing and GIS-converged technology, rather than local site analysis or instrumentation. For the site classification system (Table 1), grids combined with proxy- and V_{SZ}-based site seismic response parameters (V_{S30}, H, T_G) were developed. The site classification criteria, based on the site response parameters, divided the grids (Figure 11) based on reasonable spatial stratigraphy information and V_S. As a result, the site class-embedded grids calibrated the measured PGA by assessing the site classification and then determined F_a and F_v [10]

The spatial zonation based on H had a maximum value of approximately 45 m and a deeper distribution of more than 20 m, primarily in the coastal and adjacent plains. In areas with densely distributed residential and industrial facilities, H is usually 10 m or less. Excluding mountainous regions, V_{S30} ranged from approximately 340 to 520 m/s, with soil layer thickness ranging from approximately 180 to 240 m/s. In addition, the T_G is highest in plain and hilly areas in the center of cities with dense residential and industrial facilities, ranging from approximately 0.2 s to 0.5 s. In particular, when predicting seismic vulnerability based on the resonance potential of structures based on T_G, major sites in Gyeonggi Province exhibit a T_G distribution of approximately 0.18 to 0.49 s.

Accordingly, considering the T_G of 0.1 s for each floor of a building [7], it is possible to predict the seismic vulnerability of a facility with two to five floors in a flat area densely populated with residential and industrial facilities. For example, during the Hongseong earthquake (M_L 5.0, 1978), many of the damaged structures were three to five stories tall, with site periods in these areas ranging from approximately 0.3 to 0.5 s [17]. However, a precise prediction of the seismic vulnerability of facilities based on the relative amplification

of ground motions is possible by comprehensively comparing the T_G at the facility location, the natural period of the corresponding building (or ground-structure system), and the amplification band of the seismic wave response spectrum. Therefore, a site-specific seismic response prediction technique based on minor periodicity can be used to predict a structure's seismic vulnerability without the need for a building loss analysis using numerical techniques and fragility functions.

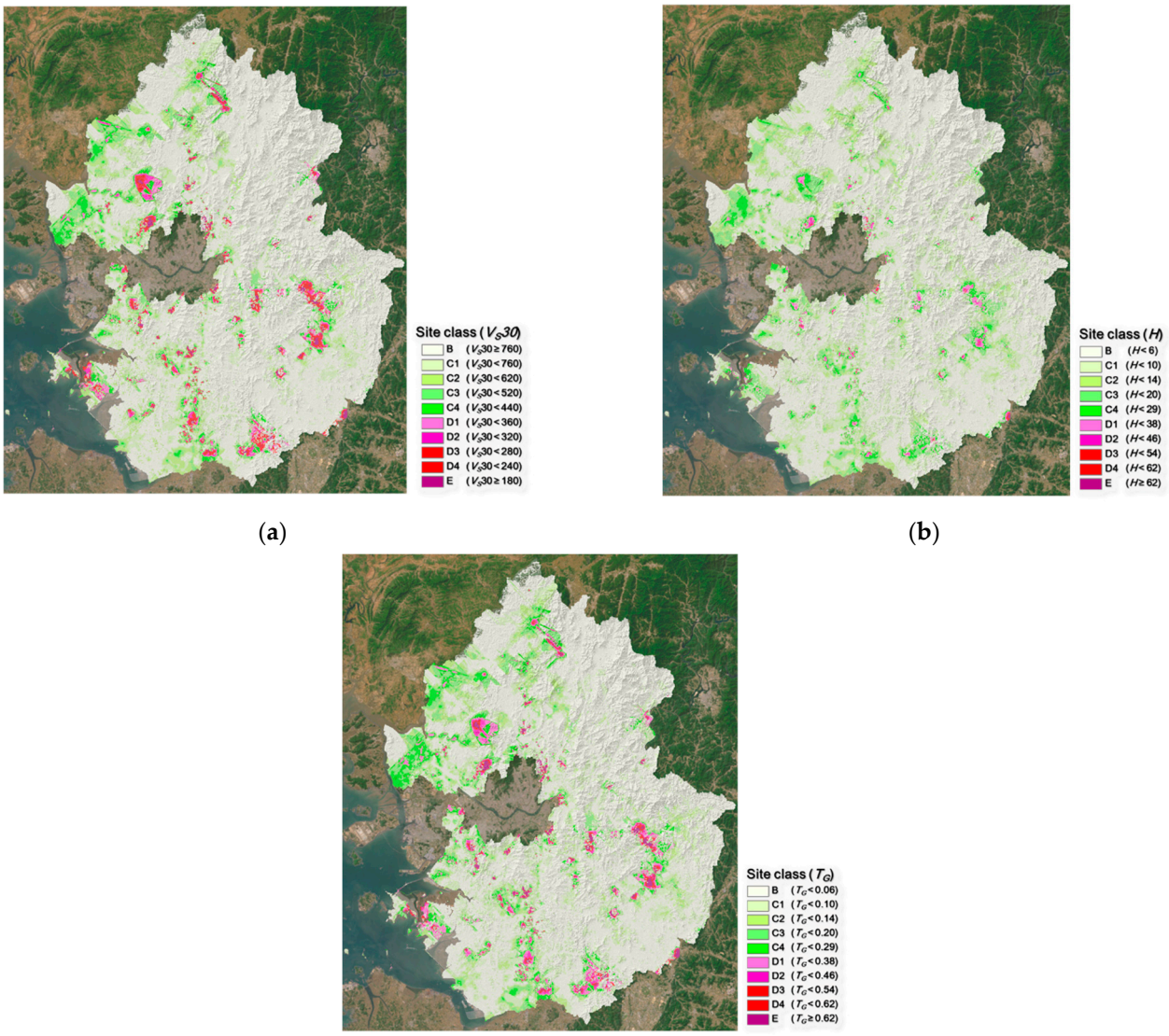


Figure 11. Spatial distribution of geotechnical grid information in Gyeonggi-do area: (**a**) V_{S30}, (**b**) H, and (**c**) T_G, by combining the spatial grid information composed of proxy-based and V_{SZ}-based grids.

Site classes D1–D3, characterized by elevations below 9 m, predominantly covered coastal and plain areas, excluding mountainous regions. The average slope measured 0.013 m/m, with a standard deviation of 0.0015 m/m. Site classes D1–D3, with an average slope of 0.005 m/m, were predominantly found in urban coastal areas, where quaternary alluvium deposits overlie thick tertiary sediments. The western and southern plains, with alluvium deposits at elevations less than 10 m, were classified as D2–E, with a slope of 0.0008 m/m.

4.4. Earthquake-Induced Landslide Hazard in Mountaneos Area

Earthquake scenarios for the Gyeonggi-do area were assessed using hazard maps based on dynamic safety factors and varying earthquake return periods. These scenarios are categorized as follows:

(a) For an earthquake with a return period of 4800 y and a PGA of 0.30 g, the susceptibility map identifies areas at high risk of landslides caused by significant seismic loads.

(b) For an earthquake return period of 2400 y and a PGA of 0.22 g, the map indicates a moderate level of landslide risk, reflecting slightly lower seismic loads.

(c) An earthquake with a return period of 1000 y and a PGA of 0.154 g indicates a lower susceptibility to landslides than the previous scenarios, with reduced seismic intensity.

(d) For an earthquake return period of 500 y and a PGA of 0.10 g, the susceptibility to landslides is further reduced, suggesting minimal risk from seismic loads.

Four PGA cases, 0.10, 0.154, 0.22, and 0.30 g, are used in the mapping of earthquake-induced landslide hazards, and the amplification factor corresponding to the amplified ShakeMap is used to calibrate the measured PGA in bedrock outcrops. In this analysis, both c and S are assumed to be zero, and γt is assumed to be 18 kN/m^2 in Equation (1) when computing the grid-based dynamic factor of safety. The Newmark displacement at the grids was calculated using the representative empirical formula (proposed by Ambraseys and Menu, 1988) (Table 2). Two specific sites were analyzed: (i) a mountainous region in Gapyeong-gun, where the risk profile may vary significantly owing to terrain characteristics, and (ii) an urban area in Suwon-si, where factors such as infrastructure and population density influence landslide hazard.

The safety factors for static and seismic slope stability on each grid were obtained using the amplified grid assembled within the slope DEM, depth of the soil layer, and internal friction angle. Figure 12 shows the results of the dynamic safety factor for four cases of different PGAs. The severity class of the dynamic factor of safety was categorized into three levels ('Low', 'Moderate', and 'High'). A factor of safety lower than one ('High' level) is common in the four cases. The area with a safety factor distribution less than one increased as the PGA increased, with a focus on the northeast mountainous regions. In addition, the area with a safety factor greater than two decreased as the PGA increased. The majority of grids with lower seismic loads (0.154 and 0.10 g) were absolutely categorized as 'Low' level (FS $\geq$ 2.0). In Gapyeong-gun's mountainous area, higher seismic loads (PGA $\geq$ 0.22) resulted in 33% of grids being classified as 'High' level (1.1 < FS $\leq$ 2.0). Otherwise, 75% of grids in the Suwon-si urban area were categorized as 'Low' level, despite PGA = 0.3 g.

Figure 13 shows the Newmark displacement results from each PGA event. The yield acceleration was calculated using the safety factor from Equation (1), and the Newmark displacement in each case was calculated using Table 2. In addition, the severity class of Newmark displacement was categorized into four levels ('Low', 'Moderate', 'High', and 'Very high'). In the case of 0.10 g, displacement of more than 99% of the area occurs within 10 mm because most of the dynamic factors of safety values in each case are greater than one, as shown in Figure 9a, and many factors in Table 1 are assumed or ignored in this analysis. On the contrary, the grid occupancy of grids classified at the 'High' and 'Very high' level, for the three cases of PGA events (0.154, 0.20, and 0.30 g) were 6, 11, and 20%, respectively. Considering the dynamic factor of safety and Newmark displacement, it is possible that the mountainous area in Gapyeong-gun can be damaged at a 'High' level (0 < FS $\leq$ 1, displacement > 50 mm) in conditions of a PGA event more than 0.22 g. Despite PGA exceeding 0.22 g at the urban area in Suwon-si, approximately 76% of grids were classified as 'Low' level (FS $\geq$ 1, displacement < 10 mm).

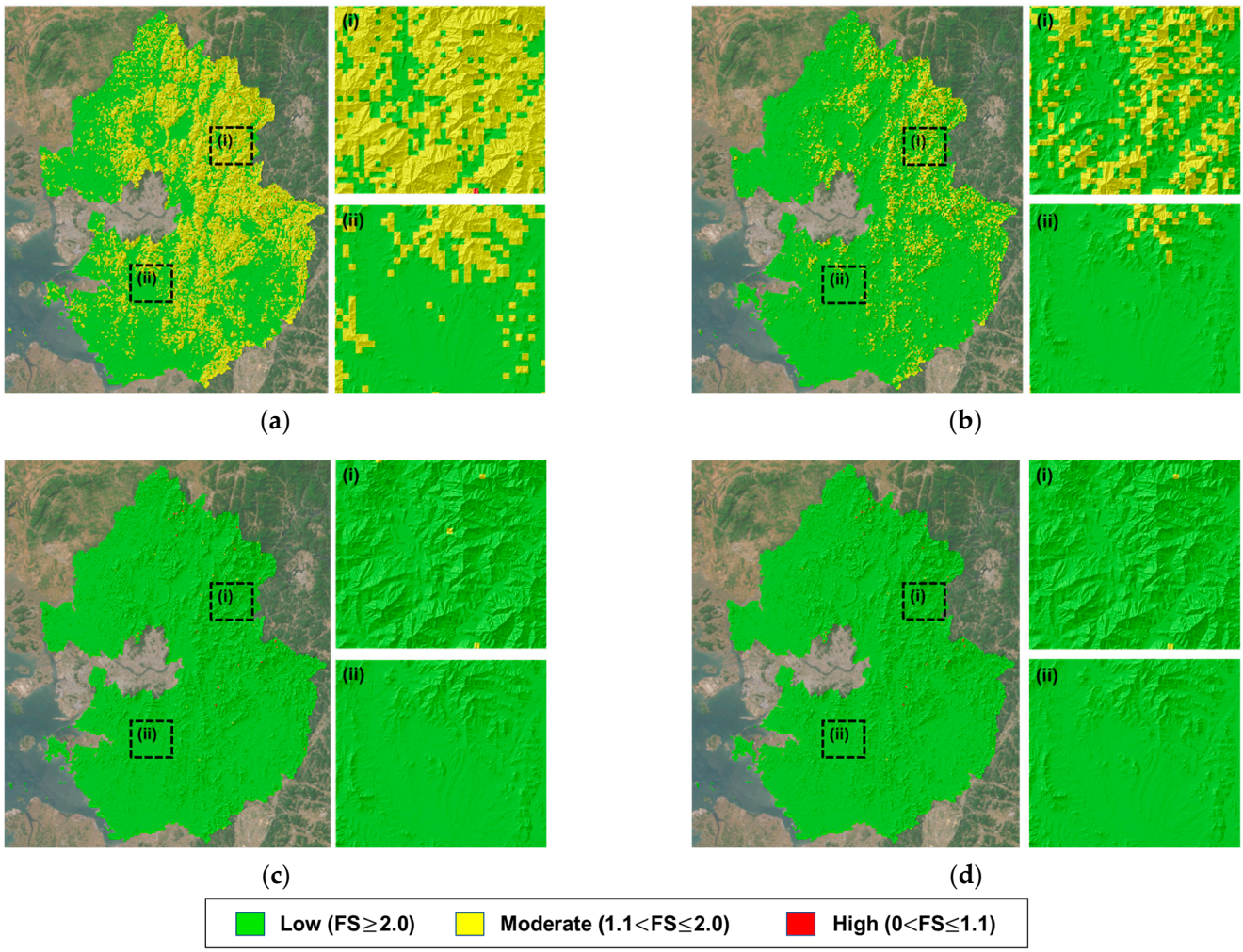


Figure 12. Earthquake-triggered landslide hazard maps defined by dynamic factor of safety for Gyeonggi-do area against (**a**) earthquake return period of 4800 y (0.30 g), (**b**) earthquake return period of 2400 y (0.22 g), (**c**) earthquake return period of 1000 y (0.154 g), and (**d**) earthquake return period of 500 y (0.10 g). Two interesting sites ((**i**) mountainous area in Gapyeong-gun; (**ii**) urban area in Suwon-si) were extended.

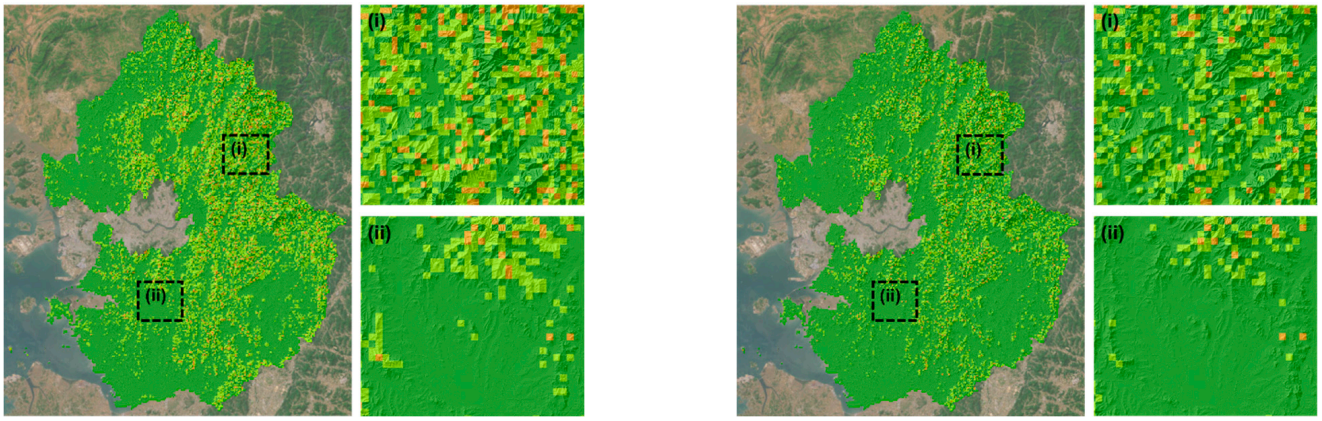


Figure 13. *Cont.*

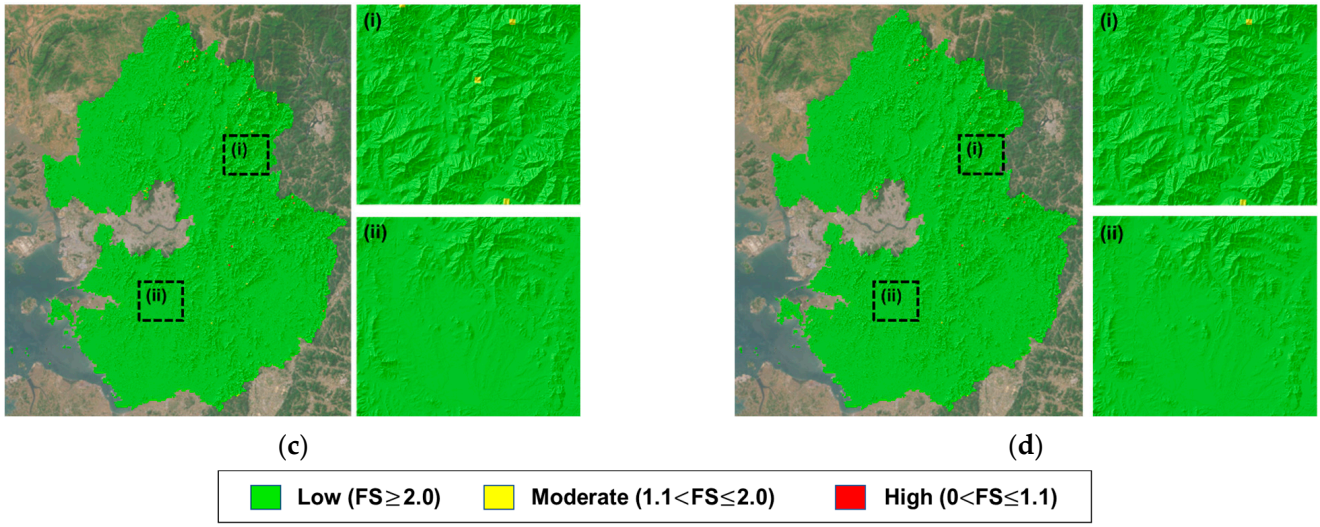


Figure 13. Earthquake-triggered landslide hazard maps defined by Newmark displacement for Gyeonggi-do area against (**a**) earthquake return period of 4800 y (0.30 g), (**b**) earthquake return period of 2400 y (0.22 g), (**c**) earthquake return period of 1000 y (0.154 g), and (**d**) earthquake return period of 500 y (0.10 g), based on the site classification map assigned with amplification factor. Two interesting sites ((**i**) mountainous area in Gapyeong-gun; (**ii**) urban area in Suwon-si) were extended.

4.5. Potential Building Damage State in Facility Area

The structural fragilities were estimated using a seismic impact analysis method based on structural fragility. The fragility curves for the building types in the registered building datasets (Figure 9d) were combined with the geotechnical grid information to compute the amplified PGA. Four earthquake scenarios were used, each with its own return periods, as well as an earthquake-induced landslide hazard assessment. Similarly, for the 2017 Pohang earthquake, the failure probabilities at the four damage levels of the unreinforced concrete structure were calculated for each building site (Figure 14). To represent the potential for structural failure according to administrative districts, a site classification map for administrative units (Si or Gu) was created by averaging the failure probability of all buildings for each of the four damage levels (slight, moderate, extensive, and complete) against four earthquake scenarios (0.10, 0.154, 0.22, and 0.30 g). Consequently, the damage state (more than 50% of failure probability) is represented using the average failure probability. Among 42 administrative districts, the 28 zones of more severe damage higher than the 'Slight' level were 30, when a PGA of 0.30 g occurred. Otherwise, the 35 zones were considered safe regions for structural fragility for an earthquake return period of 500 y and PGA of 0.10 g.

The building loss map for Suwon-si's urban area (i.e., the area shown in Figure 14) was extended across four earthquake scenarios. For PGAs below 0.154 g, 88% of the building sites were deemed safe because of the presence of non-amplifiable topsoil, such as boulder stone or silty sand. Conversely, with PGAs exceeding 0.22 g, 5% of the buildings, particularly in the western regions, were assessed as potentially damaged, including 18 unreinforced masonry structures predicted to suffer complete failure. Incorporating site-specific seismic ground amplification through geotechnical spatial grids allows the identification of damage types, such as differential settlement, by assessing zonal failure probabilities. This method is useful for immediate stabilization, restoration efforts, and post-event safety evaluations, because the complete damage level reflects the total structural failure requiring full reconstruction. Consequently, Yeongtong-gu in Suwon-si was classified at the level of complete damage.

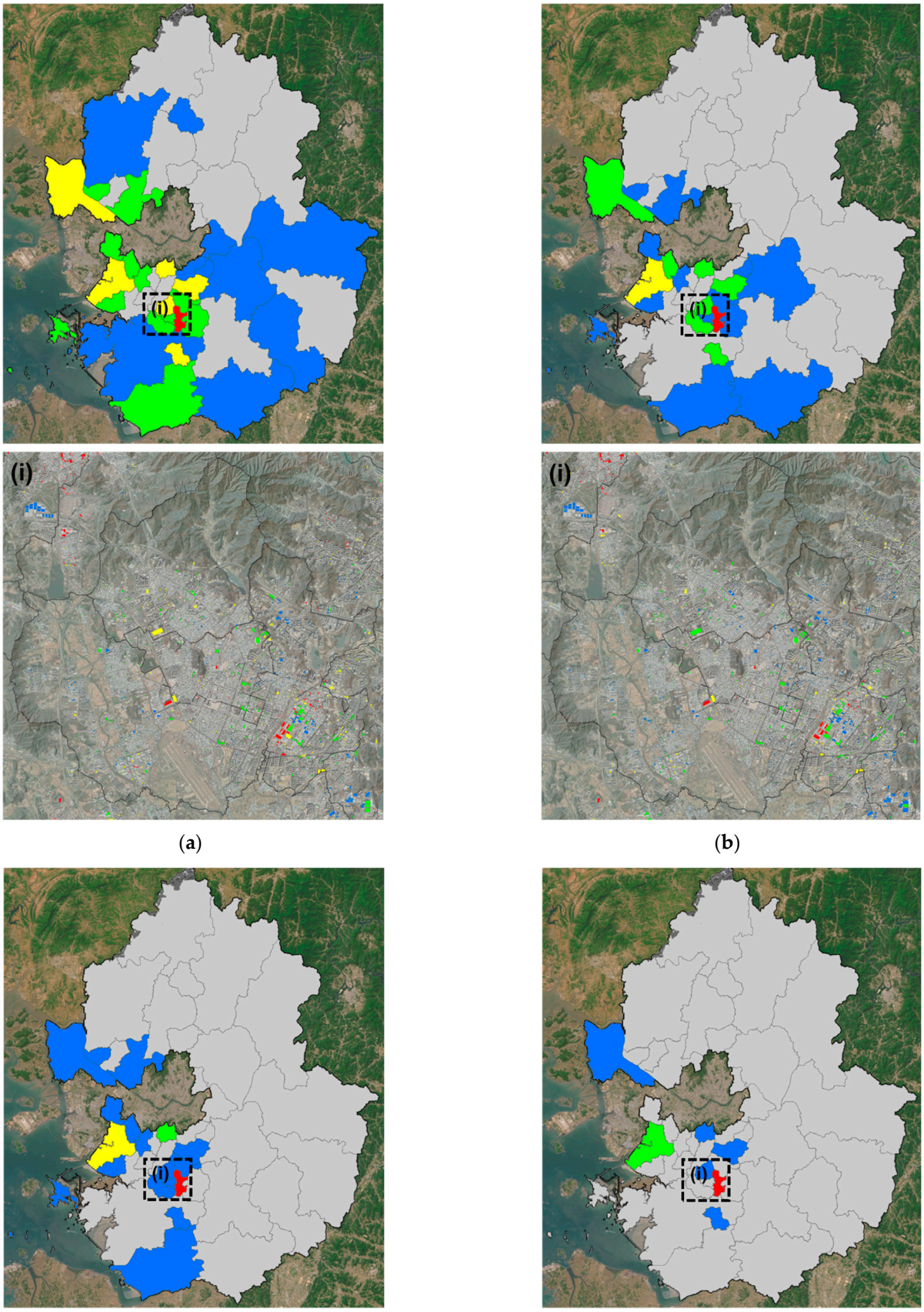


Figure 14. *Cont.*

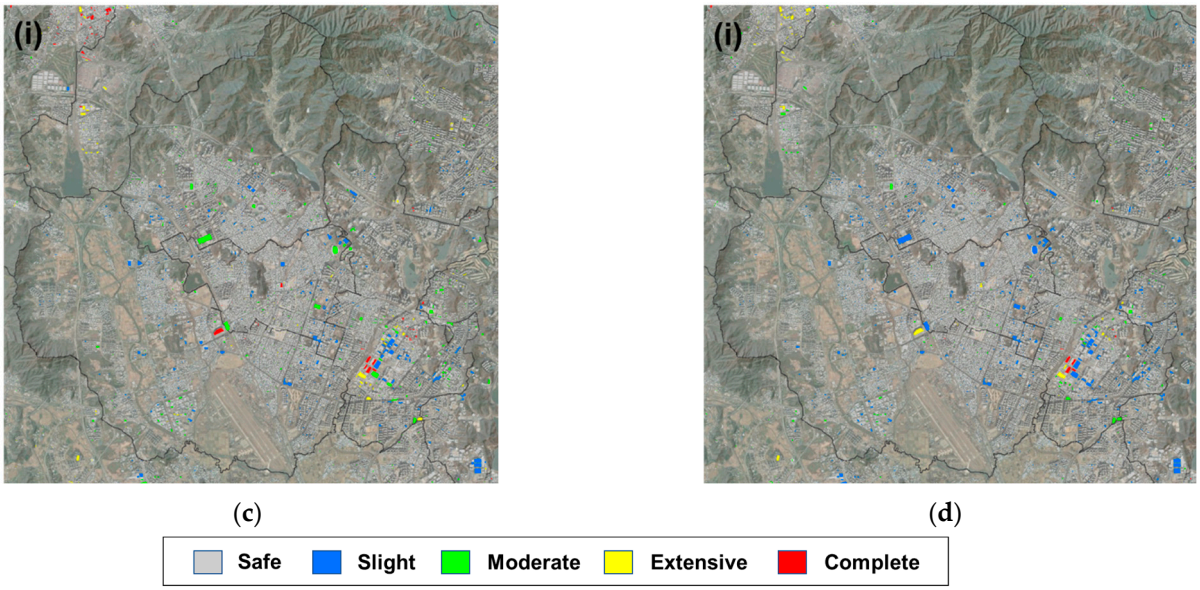


Figure 14. Site classification map for administrative unit (Si or Gu), by averaging building loss for each four damage levels (slight, moderate, extensive, and complete) against (**a**) earthquake return period of 4800 y (0.30 g), (**b**) earthquake return period of 2400 y (0.22 g), (**c**) earthquake return period of 1000 y (0.154 g), and (**d**) earthquake return period of 500 y (0.10 g). The building loss map (**i**) for urban areas in Suwon-si were extended depending on four earthquake scenarios.

5. Conclusions

Research presented in this study emphasizes the importance of conducting comprehensive seismic hazard assessments in South Korea, particularly in Gyeonggi-do Province, where urban development and geological variability pose significant risks. This study developed a multi-hazard assessment framework by integrating advanced geospatial computation techniques to address seismic impacts, landslide hazards, and structural vulnerability. The key findings indicate that the frequency of seismic events necessitates the development of site-specific seismic hazard maps, which are essential for effective urban disaster preparedness and response. The methodology used in this study, which includes the construction of geotechnical spatial grids and application of GIS-based analyses, provides a robust platform for evaluating seismic site effects and predicting potential hazards.

The framework successfully demonstrates how geostatistical methods can be used to assess ground-motion amplification and landslide risks, revealing substantial vulnerability variations based on local geological conditions. The verification of this framework, using data from the 2017 Pohang earthquake, highlights its practical applicability by showcasing the correlation between predicted and observed damage. Moreover, this study identified the significance of real-time data integration (e.g., free-filed-/structure-acceleration and displacement) through wireless networks, improving the ability to monitor seismic activity and dynamically assess structural fragility. This method not only aids in immediate response but also promotes long-term urban planning and infrastructure resilience.

In conclusion, this study emphasizes the importance of the ongoing research and development of seismic hazard assessment methodologies. South Korea can improve its preparedness for future seismic events by fostering collaboration among geotechnical engineers, urban planners, and emergency managers, ultimately safeguarding its communities and infrastructure from the devastating effects of earthquakes. The findings reveal a significant interdependence between the site-specific ground model and seismic amplification, underscoring the need for integrated hazard assessments that can enhance forecasting accuracy and improve urban resilience. By adopting this multi-hazard approach, South Korea can better mitigate economic and social losses associated with seismic events. As the goal of the study is the development of a geospatial multi-hazard assessment framework and

its applications when subjected to earthquakes, there are limitations about the uncertainty of input variables or its reliability in practical applications. In a future study, uncertainty analysis due to strength parameters and the threshold of landslide and structural fragility triggered by earthquakes will be performed.

Author Contributions: Conceptualization: Han-Saem Kim; Data curation: Han-Saem Kim; Investigation: Han-Saem Kim; Methodology: Han-Saem Kim; Writing—original draft: Han-Saem Kim; Writing—review & editing: Han-Saem Kim; Formal analysis: Mingi Kim; Funding acquisition: Mingi Kim; Project administration: Mingi Kim; Writing—review & editing: Mingi Kim. All authors have read and agreed to the published version of the manuscript.

Funding: This research received no external funding.

Data Availability Statement: The data used to support the findings of this study are available from the corresponding author upon request.

Acknowledgments: This study was supported by the Kyonggi University and Seoul Institute. And the project titled "Slope stability analysis of expressway based on GIS", funded by the Korea Expressway Corporation Research Institute.

Conflicts of Interest: The authors declare no conflicts of interest.

References

1. Sun, C.-G.; Kim, H.-S. Geostatistical assessment for the regional zonation of seismic site effects in a coastal urban area using a GIS framework. *Bull. Earthq. Eng.* **2016**, *14*, 2161–2183. [CrossRef]
2. Fang, C. SMAs for infrastructures in seismic zones: A critical review of latest trends and future needs. *J. Build. Eng.* **2022**, *57*, 104918. [CrossRef]
3. Kramer, S.L. *Geotechnical Earthquake Engineering*; Pearson Education India: Uttar Pradesh, India, 1996.
4. Borcherdt, R.D. Estimates of site-dependent response spectra for design (methodology and justification). *Earthq. Spectra* **1994**, *10*, 617–653. [CrossRef]
5. Sun, C.-G.; Chun, S.-H.; Ha, T.-G.; Chung, C.-K.; Kim, D.-S. Development and application of a GIS-based tool for earthquake-induced hazard prediction. *Comput. Geotech.* **2008**, *35*, 436–449. [CrossRef]
6. Khan, F.; Das, B.; Mishra, S.R.K.; Awasthy, M. A review on the feasibility and application of geospatial techniques in geotechnical engineering field. *Mater. Today Proc.* **2022**, *49*, 311–319. [CrossRef]
7. Kim, H.-S.; Sun, C.-G.; Cho, H.-I. Geospatial assessment of the post-earthquake hazard of the 2017 Pohang earthquake considering seismic site effects. *ISPRS Int. J. Geo-Inf.* **2018**, *7*, 375. [CrossRef]
8. Atakan, K.; Brandsdóttir, B.; Halldórsson, P.; Fridleifsson, G. Site response as a function of near-surface geology in the South Iceland seismic zone. *Nat. Hazards* **1997**, *15*, 139–164. [CrossRef]
9. Rodríguez-Marek, A.; Bray, J.D.; Abrahamson, N.A. An empirical geotechnical seismic site response procedure. *Earthq. Spectra* **2001**, *17*, 65–87. [CrossRef]
10. Sun, C.-G.; Kim, D.-S.; Chung, C.-K. Geologic site conditions and site coefficients for estimating earthquake ground motions in the inland areas of Korea. *Eng. Geol.* **2005**, *81*, 446–469. [CrossRef]
11. Poggi, V.; Burjanek, J.; Michel, C.; Fäh, D. Seismic site-response characterization of high-velocity sites using advanced geophysical techniques: Application to the NAGRA-Net. *Geophys. J. Int.* **2017**, *210*, 645–659. [CrossRef]
12. Olabode, O.P.; San, L.H. Analysis of soil electrical resistivity and hydraulic conductivity relationship for characterisation of lithology inducing slope instability in residual soil. *Int. J. Geo-Eng.* **2023**, *14*, 7. [CrossRef]
13. Mankelow, J.M.; Murphy, W. Using GIS in the probabilistic assessment of earthquake triggered landslide hazards. *J. Earthq. Eng.* **1998**, *2*, 593–623. [CrossRef]
14. Lin, M.-L.; Tung, C.-C. A GIS-based potential analysis of the landslides induced by the Chi-Chi earthquake. *Eng. Geol.* **2004**, *71*, 63–77. [CrossRef]
15. Arrais, S.; Urquiza-Aguiar, L.; Tripp-Barba, C. Analysis of information availability for seismic and volcanic monitoring systems: A review. *Sensors* **2022**, *22*, 5186. [CrossRef]
16. Khedo, K.K.; Bissessur, Y.; Goolaub, D.S. An inland Wireless Sensor Network system for monitoring seismic activity. *Futur. Gener. Comput. Syst.* **2020**, *105*, 520–532. [CrossRef]
17. Sun, C.-G.; Kim, H.-S. GIS-based regional assessment of seismic site effects considering the spatial uncertainty of site-specific geotechnical characteristics in coastal and inland urban areas. *Geomat. Nat. Hazards Risk* **2017**, *8*, 1592–1621. [CrossRef]
18. Khan, A.A. Geophysical characterization and earthquake hazard vulnerability of Dhaka Mega City, Bangladesh, vis-à-vis impact of scenario earthquakes. *Nat. Hazards* **2016**, *82*, 1147–1166. [CrossRef]
19. Lombardo, L.; Bakka, H.; Tanyas, H.; van Westen, C.; Mai, P.M.; Huser, R. Geostatistical modeling to capture seismic-shaking patterns from earthquake-induced landslides. *J. Geophys. Res. Earth Surf.* **2019**, *124*, 1958–1980. [CrossRef]

20. Kim, H.-S.; Sun, C.-G.; Cho, H.-I. Geospatial big data-based geostatistical zonation of seismic site effects in Seoul metropolitan area. *ISPRS Int. J. Geo-Inf.* **2017**, *6*, 174. [CrossRef]
21. Kim, H.-S.; Chung, C.-K. Integrated system for site-specific earthquake hazard assessment with geotechnical spatial grid information based on GIS. *Nat. Hazards* **2016**, *82*, 981–1007. [CrossRef]
22. Zheng, W.; Luna, R. Nonlinear site response and liquefaction analysis in the New Madrid seismic zone. *Geotech. Geol. Eng.* **2011**, *29*, 463–475. [CrossRef]
23. Kircher, C.A.; Reitherman, R.K.; Whitman, R.V.; Arnold, C. Estimation of earthquake losses to buildings. *Earthq. Spectra* **1997**, *13*, 703–720. [CrossRef]
24. Sun, C.-G.; Kim, H.-S.; Chung, C.-K.; Chi, H.-C. Spatial zonations for regional assessment of seismic site effects in the Seoul metropolitan area. *Soil Dyn. Earthq. Eng.* **2014**, *56*, 44–56. [CrossRef]
25. Govindaraju, L.; Bhattacharya, S. Site-specific earthquake response study for hazard assessment in Kolkata city, India. *Nat. Hazards* **2012**, *61*, 943–965. [CrossRef]
26. Roy, N.; Sahu, R. Site specific ground motion simulation and seismic response analysis for microzonation of Kolkata. *Geomech. Eng.* **2012**, *4*, 1–18. [CrossRef]
27. Pitilakis, K.; Crowley, H.; Kaynia, A.M. SYNER-G: Typology definition and fragility functions for physical elements at seismic risk. *Geotech. Geol. Earthq. Eng.* **2014**, *27*, 1–28.
28. Bazzurro, P.; Cornell, C.A. Ground-motion amplification in nonlinear soil sites with uncertain properties. *Bull. Seismol. Soc. Am.* **2004**, *94*, 2090–2109. [CrossRef]
29. Vilanova, S.P.; Fonseca, J.F.B.D. Probabilistic seismic-hazard assessment for Portugal. *Bull. Seism. Soc. Am.* **2007**, *97*, 1702–1717. [CrossRef]
30. Kim, H.-S.; Sun, C.-G.; Lee, M.-G.; Cho, H.-I. Terrain proxy-based site classification for seismic zonation in North Korea within a geospatial data-driven workflow. *Remote Sens.* **2021**, *13*, 1844. [CrossRef]
31. Dobry, R.; Borcherdt, R.D.; Crouse, C.B.; Idriss, I.M.; Joyner, W.B.; Martin, G.R.; Power, M.S.; Rinne, E.E.; Seed, R.B. New site coefficients and site classification system used in recent building seismic code provisions. *Earthq. Spectra* **2000**, *16*, 41–67. [CrossRef]
32. McPherson, A.; Hall, L. Site classification for earthquake hazard and risk assessment in Australia. *Bull. Seism. Soc. Am.* **2013**, *103*, 1085–1102. [CrossRef]
33. Moore, I.D.; Grayson, R.B. Terrain-based catchment partitioning and runoff prediction using vector elevation data. *Water Resour. Res.* **1991**, *27*, 1177–1191. [CrossRef]
34. Cai, Z.; Bathurst, R. Deterministic sliding block methods for estimating seismic displacements of earth structures. *Soil Dyn. Earthq. Eng.* **1996**, *15*, 255–268. [CrossRef]
35. United States Navy. *Design Manual 7.01*; NAVFAC DM-7.1; United States Navy: Alexandria, VA, USA, 1982.
36. Peck, R.B.; Hanson, W.E.; Thornburn, T.H. *Foundation Engineering*, 2nd ed.; Wiley: New York, NY, USA, 1974.
37. Ambraseys, N.N.; Menu, J.A.M. Earthquake-induced ground displacements. *Earthq. Eng. Struct. Dyn.* **1988**, *16*, 985–1006. [CrossRef]
38. Shinozuka, M.; Feng, M.Q.; Kim, H.-K.; Kim, S.-H. Nonlinear static procedure for fragility curve development. *J. Eng. Mech.* **2000**, *126*, 1287–1295. [CrossRef]
39. Cornell, C.A.; Jalayer, F.; Hamburger, R.O.; Foutch, D.A. Probabilistic basis for 2000 SAC federal emergency management agency steel moment frame guidelines. *J. Struct. Eng.* **2002**, *128*, 526–533. [CrossRef]
40. Gardoni, P.; Der Kiureghian, A.; Mosalam, K.M. Probabilistic capacity models and fragility estimates for reinforced concrete columns based on experimental observations. *J. Eng. Mech.* **2002**, *128*, 1024–1038. [CrossRef]
41. Au, S.K.; Beck, J.L. Subset Simulation and its application to seismic risk based on dynamic analysis. *J. Eng. Mech.* **2003**, *129*, 901–917. [CrossRef]
42. Schotanus, M.; Franchin, P.; Lupoi, A.; Pinto, P. Seismic fragility analysis of 3D structures. *Struct. Saf.* **2004**, *26*, 421–441. [CrossRef]
43. Lupoi, G.; Calvi, G.M.; Lupoi, A.; Pinto, P.E. Comparison of different approaches for seismic assessment of existing buildings. *J. Earthq. Eng.* **2004**, *8*, 121–160. [CrossRef]
44. Kiureghian, A.D. A coherency model for spatially varying ground motions. *Earthq. Eng. Struct. Dy-Namics.* **1996**, *25*, 99–111. [CrossRef]
45. Pinto, P.E.; Franchin, P.; Lupoi, A.; Lupoi, G. Seismic fragility analysis of structural systems. In Proceedings of the International Workshop on Performance Based Design, Bled, Slovenia, 28 June–1 July 2004.
46. Huang, Y.; Yu, M.; Huang, Y.; Yu, M. Macroscopic Characteristics of Seismic Liquefaction. *Hazard Anal. Seism. Soil Liq.* **2017**, 11–33. [CrossRef]
47. Jalayer, F.; Asprone, D.; Prota, A.; Manfredi, G. A decision support system for post-earthquake reliability assessment of structures subjected to aftershocks: An application to L'Aquila earthquake, 2009. *Bull. Earthq. Eng.* **2010**, *9*, 997–1014. [CrossRef]
48. Kang, S.; Kim, B.; Bae, S.; Lee, H.; Kim, M. Earthquake-induced ground deformations in the low-seismicity region: A case of the 2017 M5.4 Pohang, South Korea, earthquake. *Earthq. Spectra* **2019**, *35*, 1235–1260. [CrossRef]
49. Fadhillah, M.F.; Lee, C.W. The estimated source of 2017 Pohang earthquake using surface deformation modeling based on multi-frequency InSAR data. *Korean J. Remote Sens.* **2021**, *37*, 57–67.

50. Rose, A.; Porter, K.; Dash, N.; Bouabid, J.; Huyck, C.; Whitehead, J.; Shaw, D.; Eguchi, R.; Taylor, C.; McLane, T.; et al. Benefit-cost analysis of FEMA hazard mitigation grants. *Nat. Hazards Rev.* **2007**, *8*, 97–111. [CrossRef]
51. Ray, P.; Manach, Y.L.; Riou, B.; Houle, T.T.; Warner, D.S. Statistical evaluation of a biomarker. *J. Am. Soc. Anesthesiol.* **2010**, *112*, 1023–1040. [CrossRef]
52. Kim, H.-S.; Chung, C.-K.; Kim, J.-J. Three-dimensional geostatistical integration of borehole and geophysical datasets in developing geological unit boundaries for geotechnical investigations. *Q. J. Eng. Geol. Hydrogeol.* **2018**, *51*, 79–95. [CrossRef]

Disclaimer/Publisher's Note: The statements, opinions and data contained in all publications are solely those of the individual author(s) and contributor(s) and not of MDPI and/or the editor(s). MDPI and/or the editor(s) disclaim responsibility for any injury to people or property resulting from any ideas, methods, instructions or products referred to in the content.